The Indium and Zinc Mediated Acyloxyallylation of Protected and Unprotected Aldotetroses – Revealing a Pronounced Diastereodivergence and a Fundamental Difference in the Performance of the Mediating Metal

Markus Draskovits[1], Christian Stanetty[1,*], Ian R. Baxendale[2], Marko D. Mihovilovic[1]

[1]Institute of Applied Synthetic Chemistry, TU Wien, Getreidemarkt 9, 1060 Vienna, Austria
[2]Department of Chemistry, Durham University, South Road, Durham, DH1 3LE, United Kingdom
*E-mail: christian.stanetty@tuwien.ac.at

Part 1: Quantification of threose derived enitols

Part 2: Investigation of the fate of bromopropenyl esters 3a and 23 under the reaction conditions

Part 3: ^{1}H and ^{13}C-NMRs of the synthesized compounds

Part 1: Quantification of threose derived enitols

Figure S1. Determination of the enitol-ratio **17a-d** (*gulo*>*ido*>*talo* as peracetates) from D-threose **14**[1]

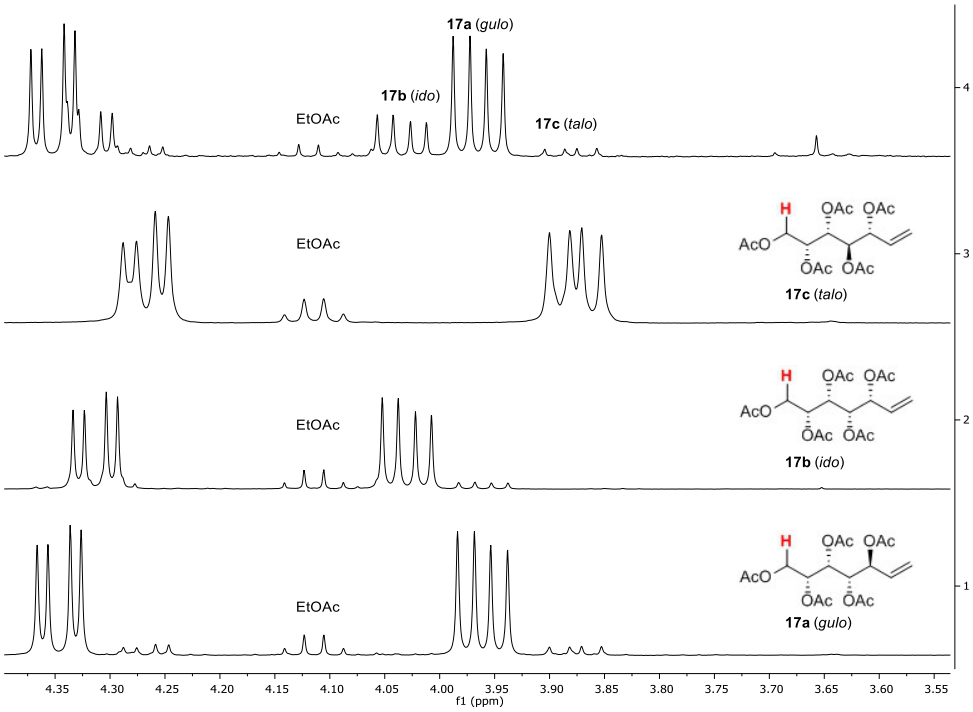

Figure S2. Determination of enitole-ratio **16a-d** (*talo*>*galacto*>*gulo*) derived from protected D-threose **15**[2]

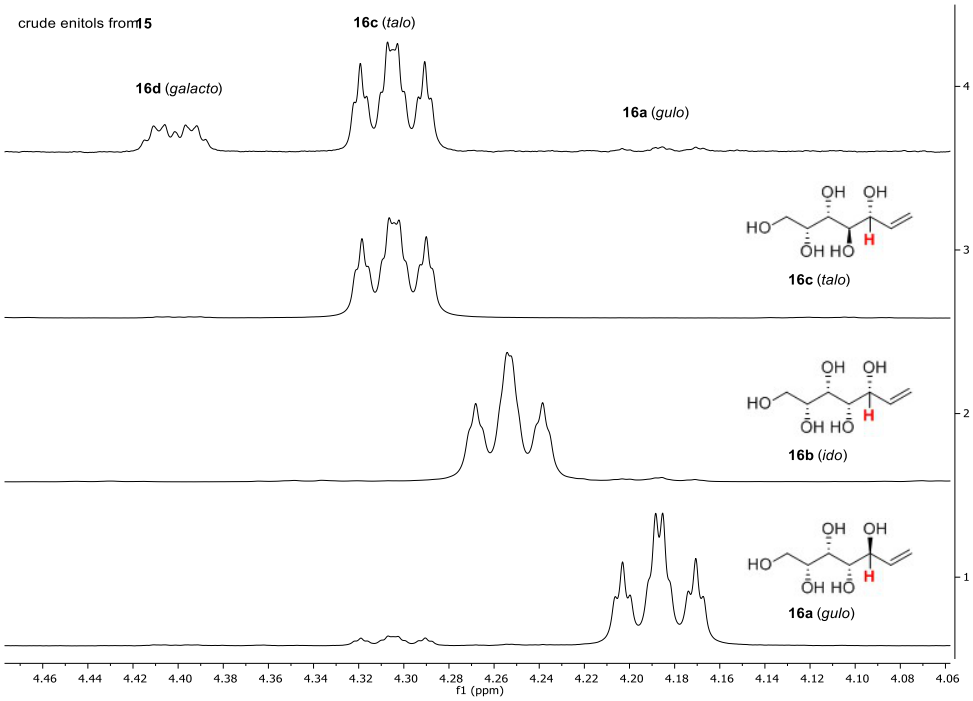

[1] based on integration of the diagnostic H7b-signals

[2] based on the integration of the diagnostic allylic position H3.

Part 2: **Investigation of the fate of bromopropenyl esters 3a and 23 under the reaction conditions**

To mimic the reaction conditions in anhydrous EtOH we followed the fate of bromopropenyl acetate **3a** in MeOH-d_4 (without indium) at rt over time (^{1}H-NMR). An immediate and rapid consumption of reagent **3a** (*E*-isomer faster than *Z*-isomer) and a clean formation of **25** (judged by the concomitant formation of d3-methylacetate in amounts equal to consumed **3a**) was observed, putatively *via* the transient intermediate **24**. Intermediate **25** was then converted in a slower manner to 1,1,2 trimethoxy propane **26-d$_{10}$** with deuterium-incorporation at the 2-position. Concomitant to the initial formation of intermediate **21** a significant shift of the HDO signal was observed which remained unaltered by the conversion to the final compound **26-d$_{10}$**. This observation is consistent with the drop of pH which was reported before and also observed by us.

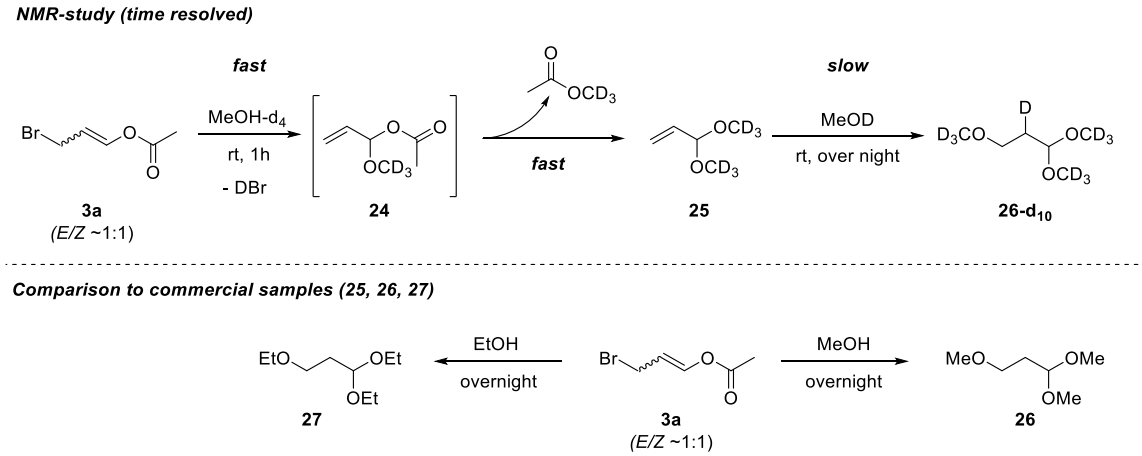

*Scheme S1: Fate of bromopropenylacetate **3a** in alcoholic solutions (NMR and isolation)*

To confirm the above interpretation of the NMR-study in terms of final product, analogous experiments in non-deuterated MeOH and EtOH were performed giving 1,1,2 trimethoxy propane **26** and 1,1,2-triethoxypropane **27** upon evaporation, clarifying that the acetyl group is not incorporated in the final product (not clear from the NMR-study). Subjection of the more stable chloropropenyl pivaloate **23** to the same conditions in MeOH-d_4 gave analogous but significantly slower conversion in the first step, in particular of the (*Z*)-isomer which was still present after 36h. The intermediate **25** was consequently only detected in minor amounts but the final product formed was the same compound **26-d$_{10}$**, further supporting our postulated order of events.

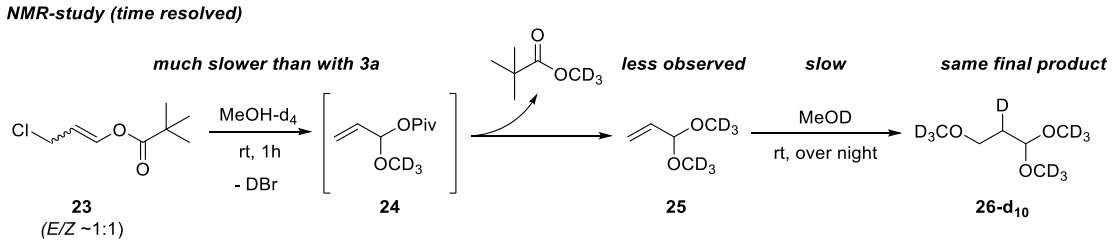

*Scheme S2: Fate of chloropropenyl pivaloate **23** in solution of MeOH-d4 in comparison to **3a***

Figure S3. Time resolved conversion of **3a** to **26-d$_{10}$** via the rapidly formed intermediates **25**.[3]

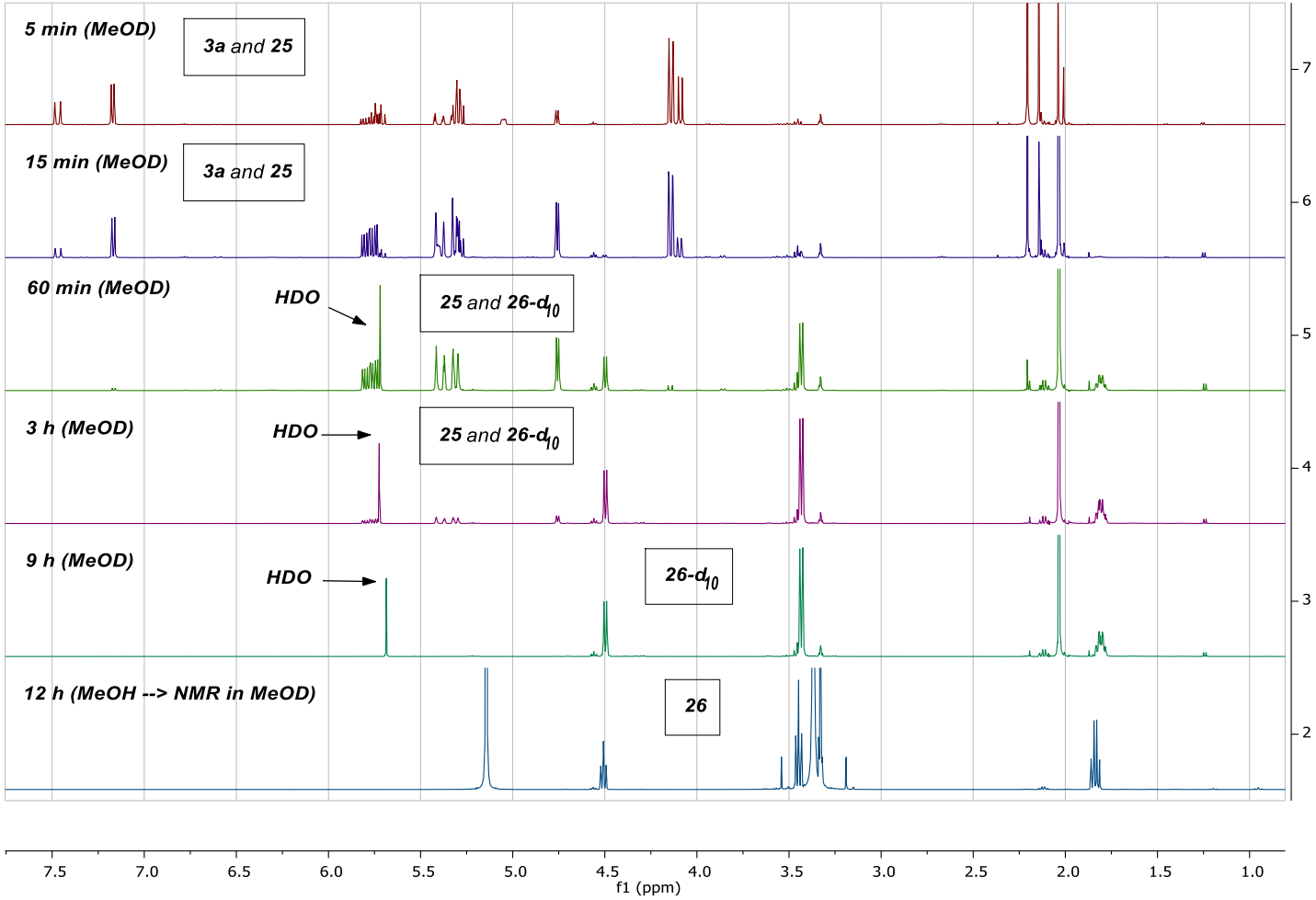

[3] Noteworthy, the comparison with isolated **26** (bottom) reveals the missing ^{3}J-couplings (4.5 ppm, 3.4 ppm) and additional small couplings (1.8) due to the tentative incorporation of deuterium in **26-d$_{10}$**.

Figure S4. Conversion of **23** to **26-d$_{10}$** and comparison with isolated **26-d$_{10}$** from the experiment with **3a** (bottom)

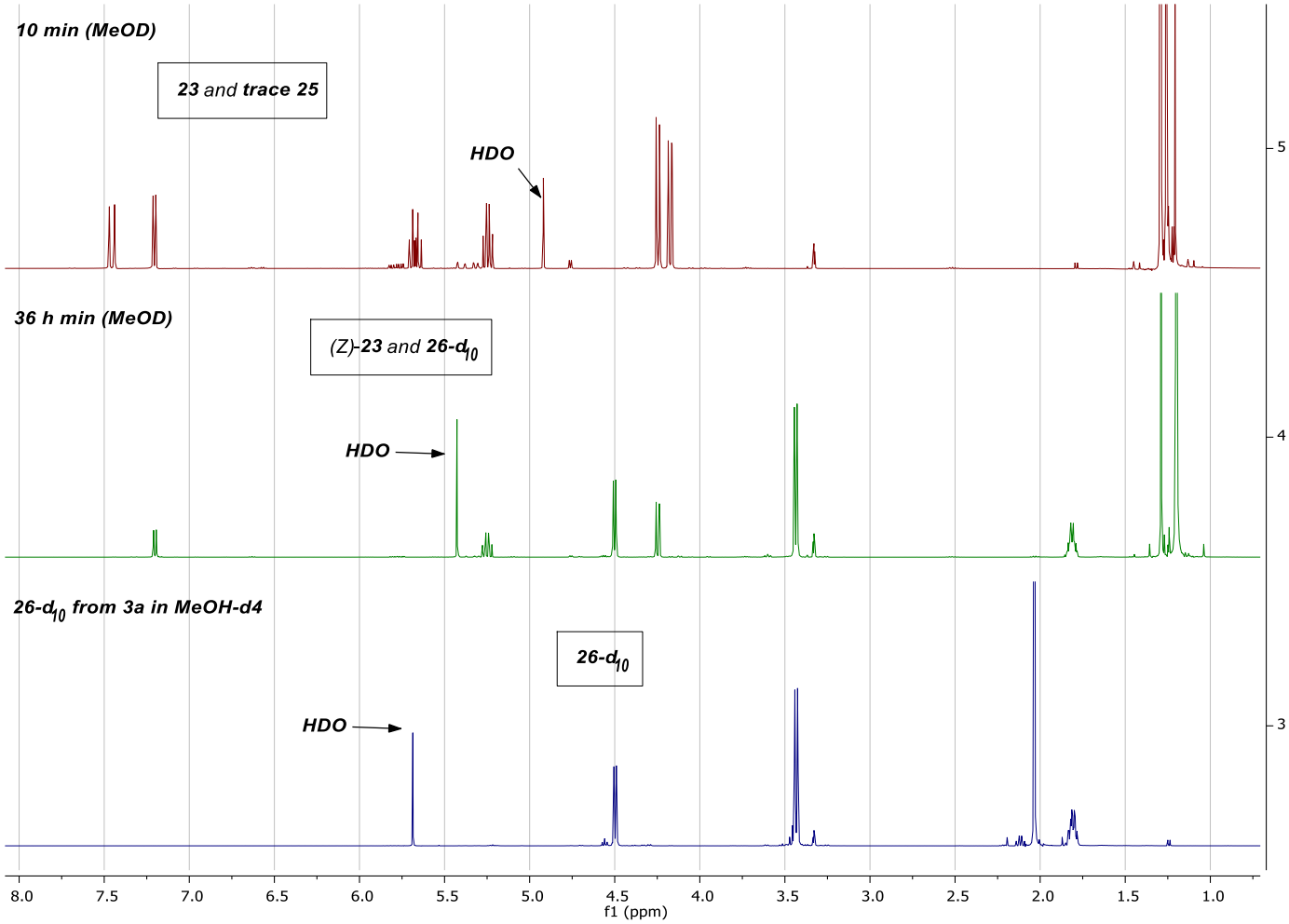

Part 3: ^{1}H and ^{13}C-NMRs of synthesized compounds

Figure S5. ^{1}H-NMR (400 MHz, $CDCl_3$) of **3c**

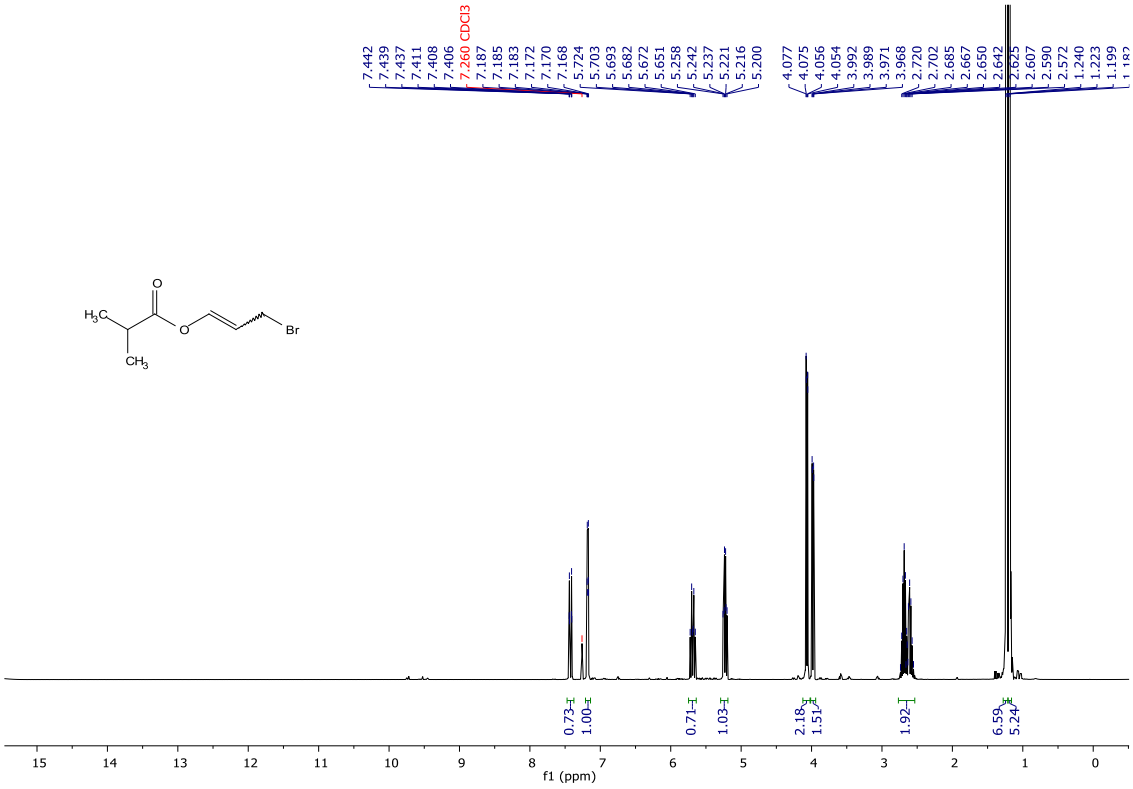

Figure S6. ^{13}C-NMR (101 MHz, $CDCl_3$) of **3c**

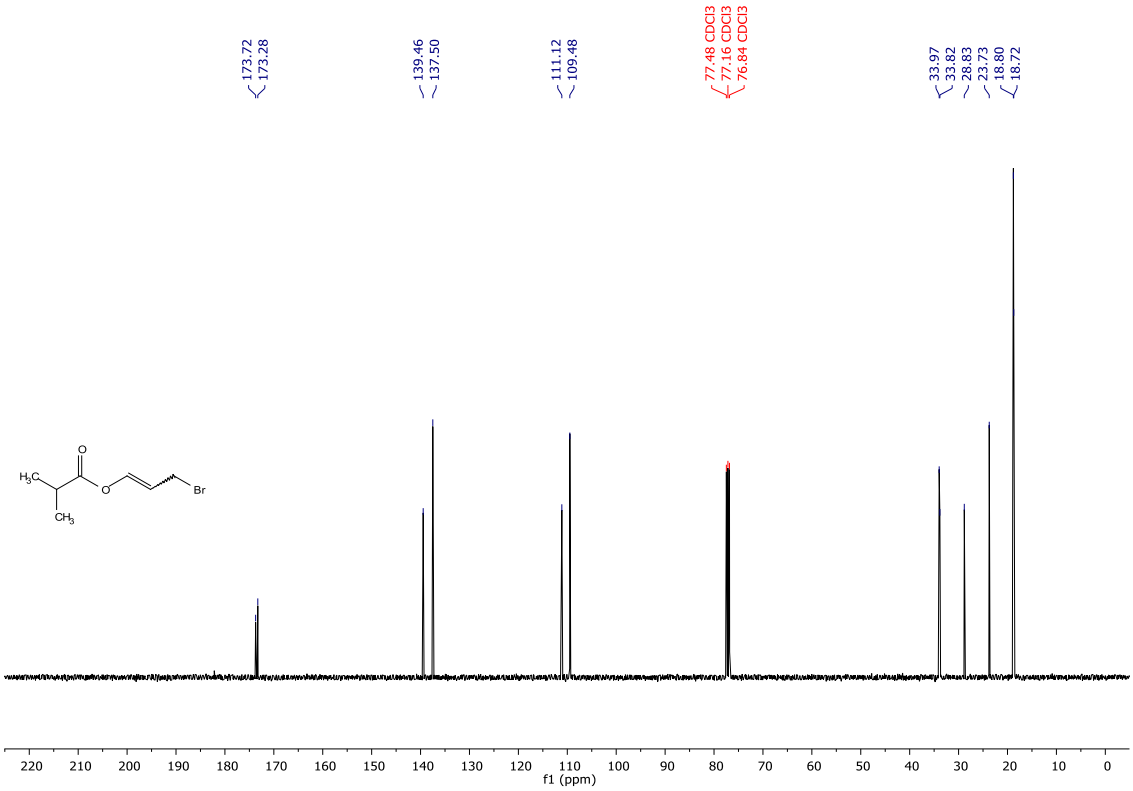

Figure S7. ^{1}H-NMR (400 MHz, $CDCl_3$) of **3d**

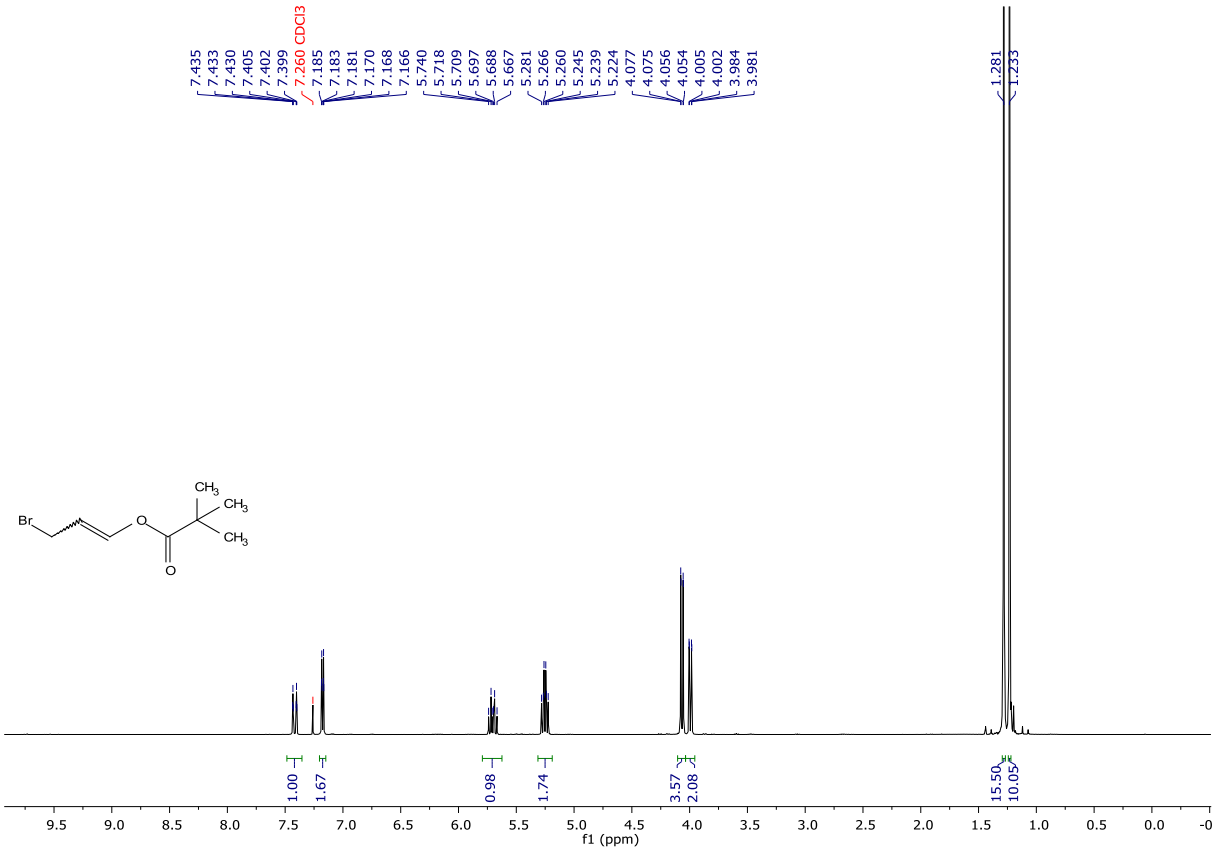

Figure S8. ^{13}C-NMR (101 MHz, $CDCl_3$) of **3d**

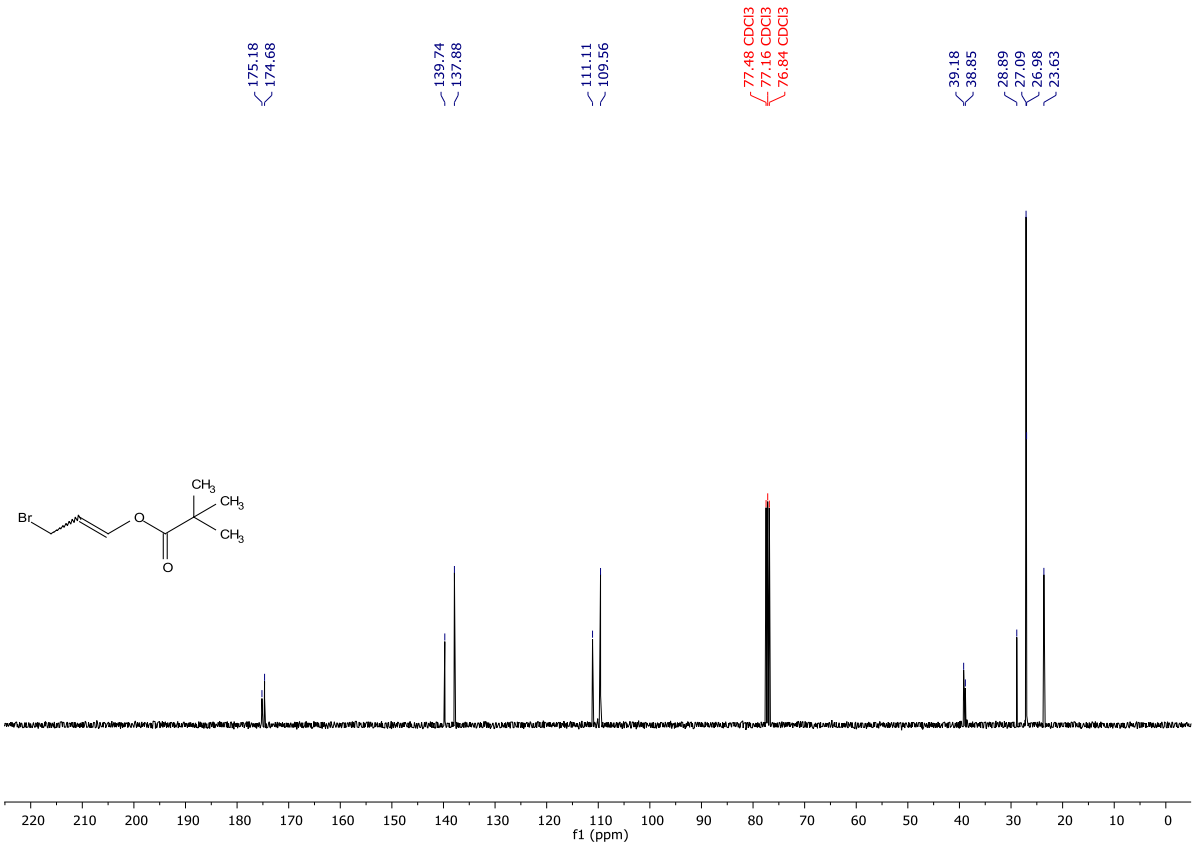

Figure S9. ^{1}H-NMR (400 MHz, D_2O) of **6**

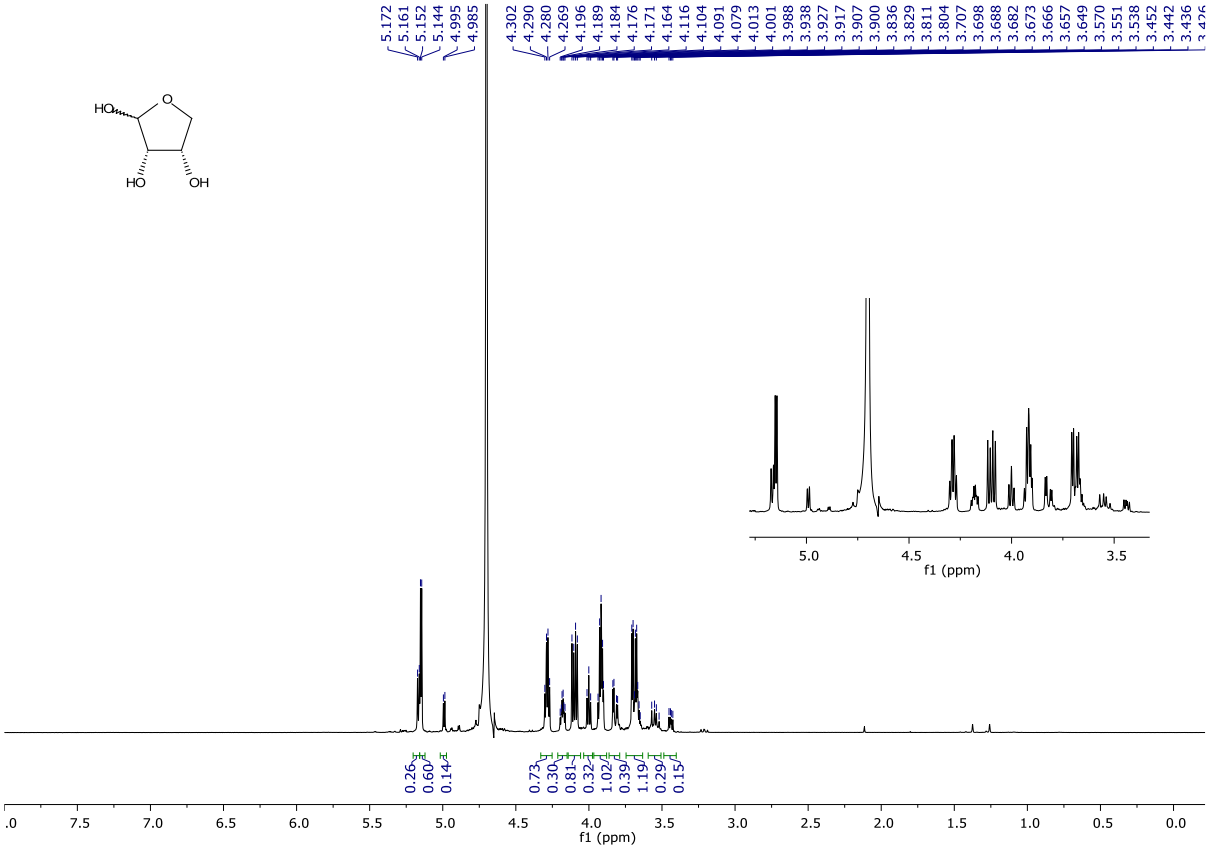

Figure S10. ^{13}C-NMR (101 MHz, D_2O) of **6**

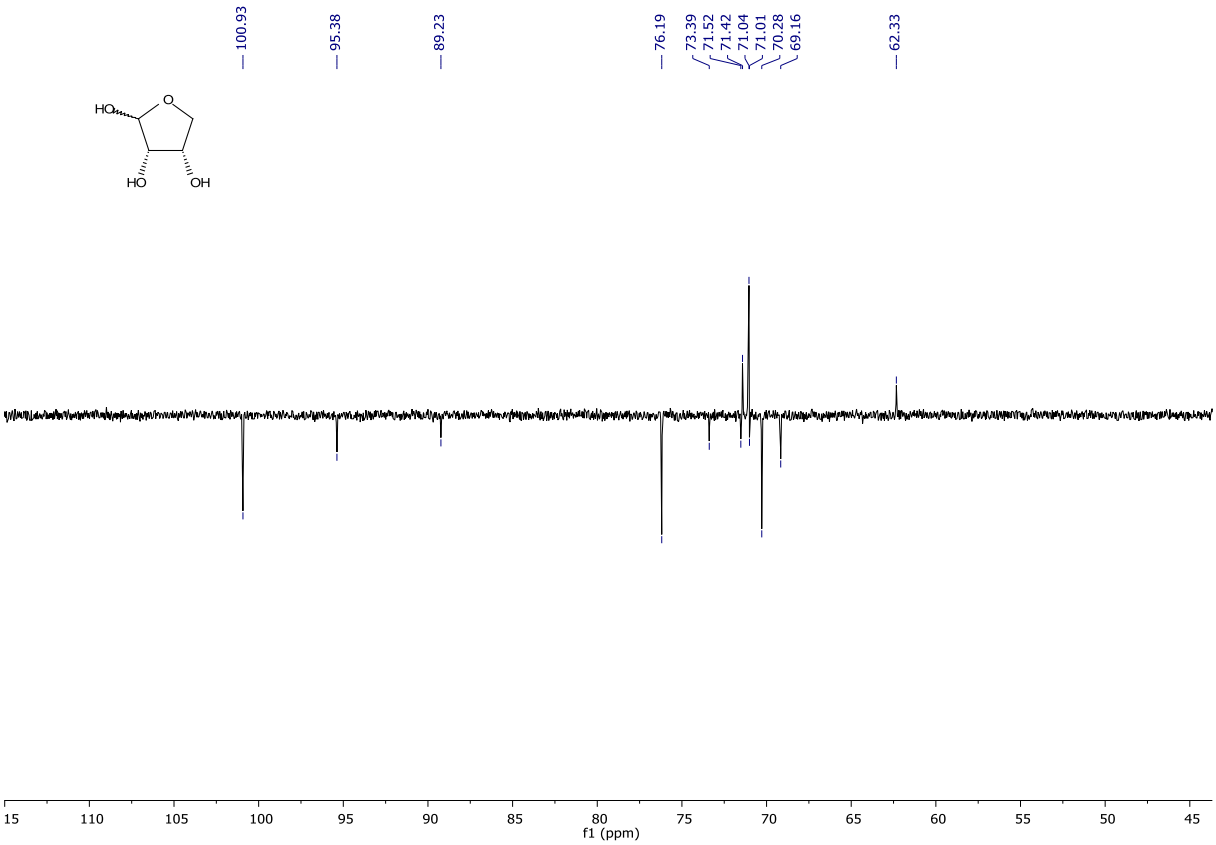

Figure S11. ^{1}H-NMR (400 MHz, $CDCl_3$) of **7**

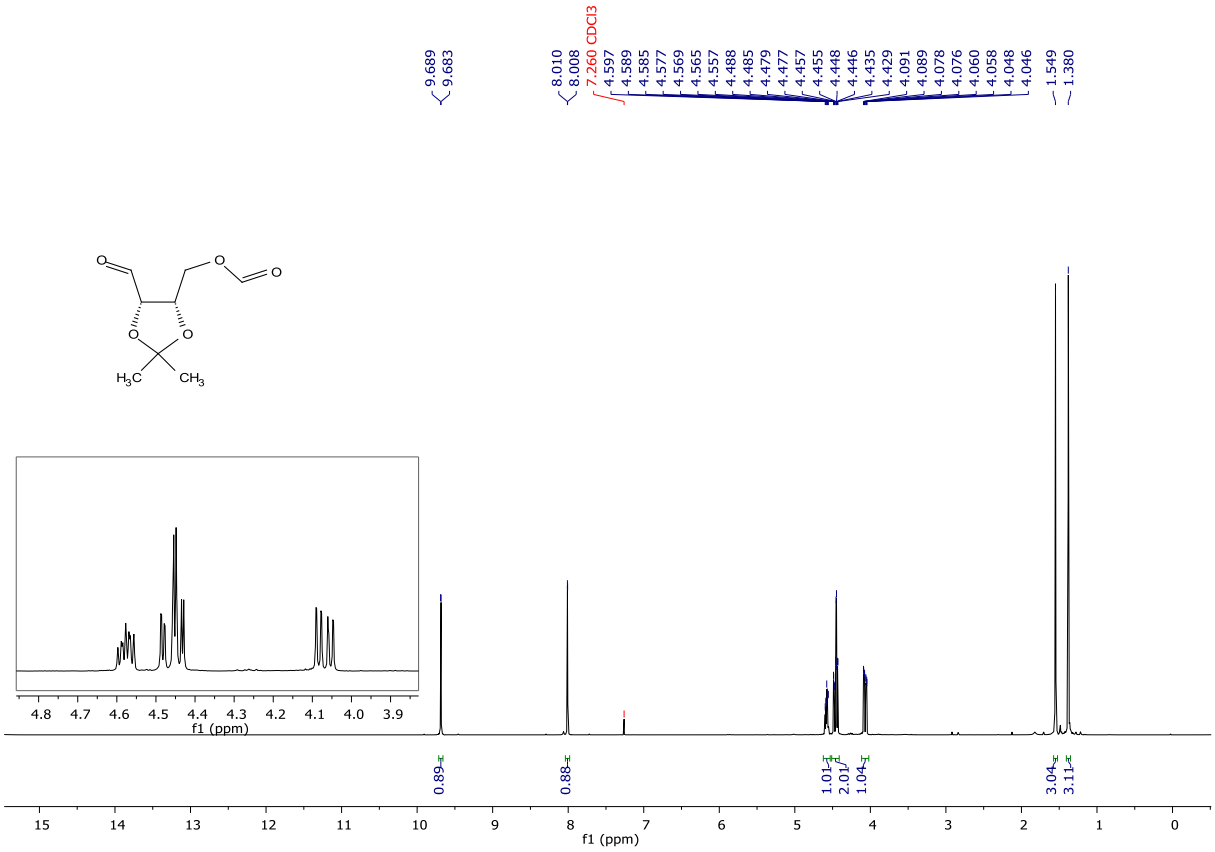

Figure S12. ^{13}C-NMR (101 MHz, $CDCl_3$) of **7**

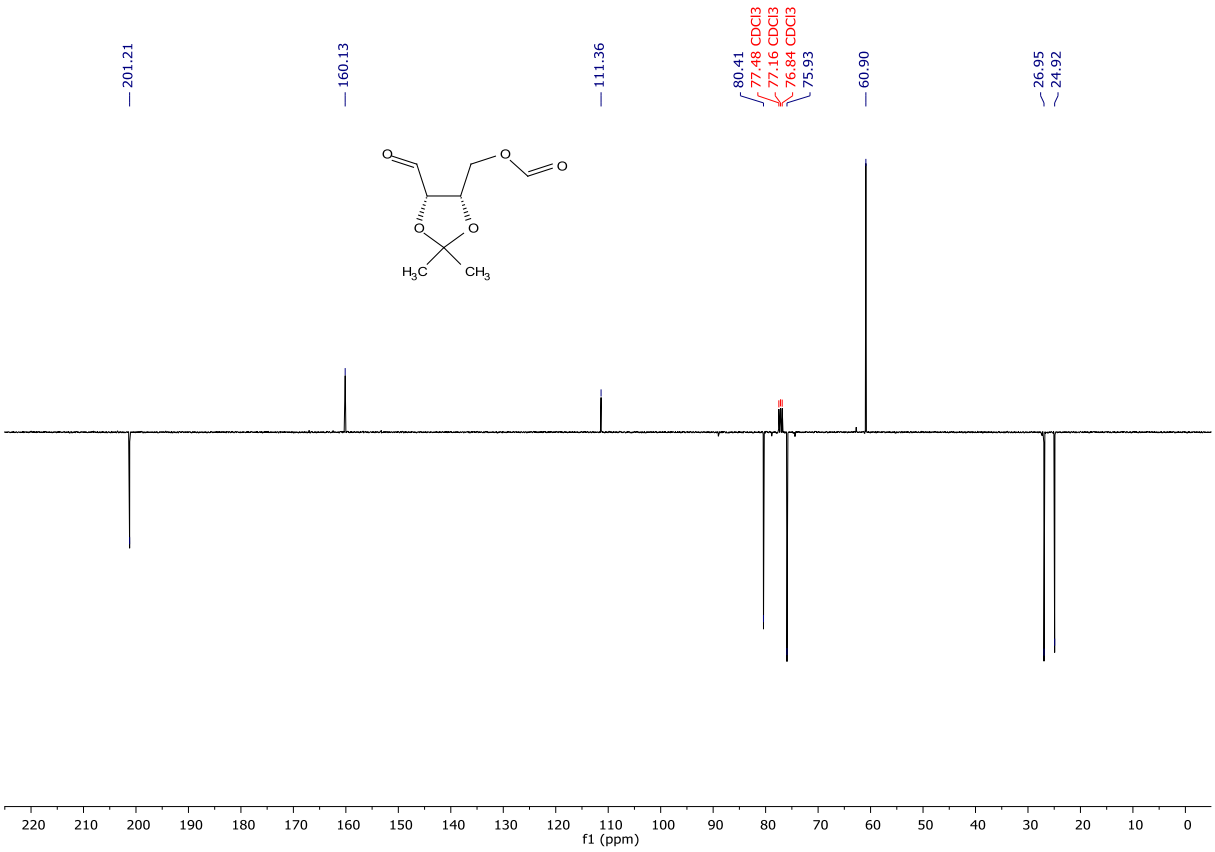

Figure S13. ^{1}H-NMR (400 MHz, MeOD) of **8a**

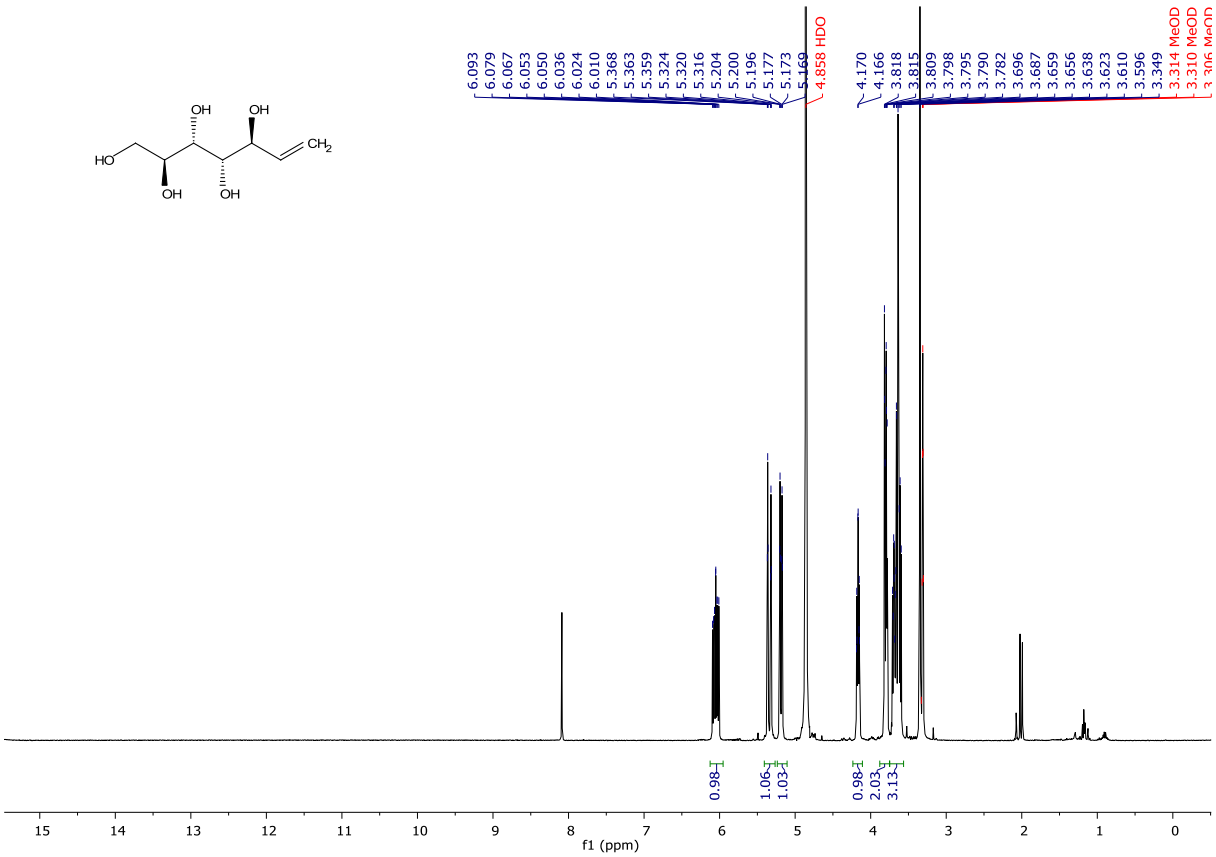

Figure S14. ^{13}C-NMR (101 MHz, MeOD) of **8a**

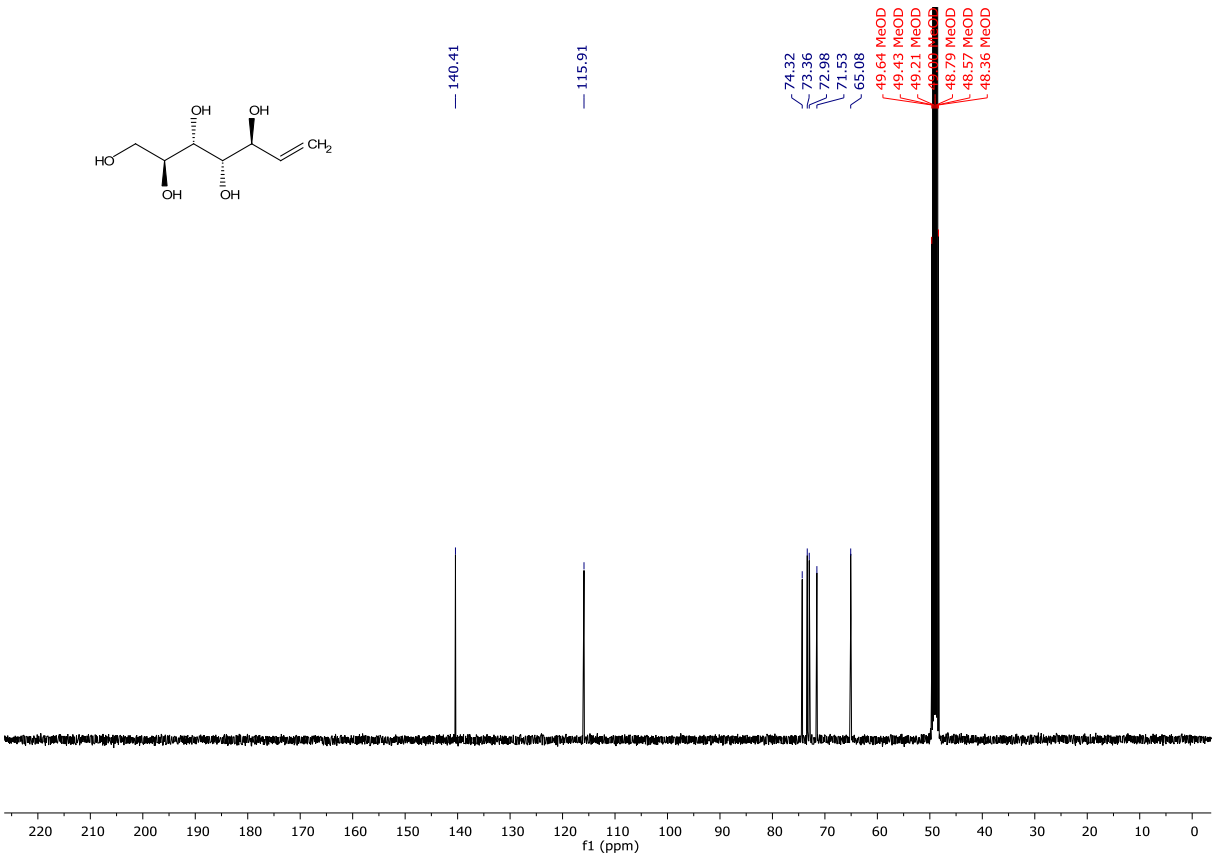

Figure S15. ^{1}H-NMR (400 MHz, MeOD) of **8b**

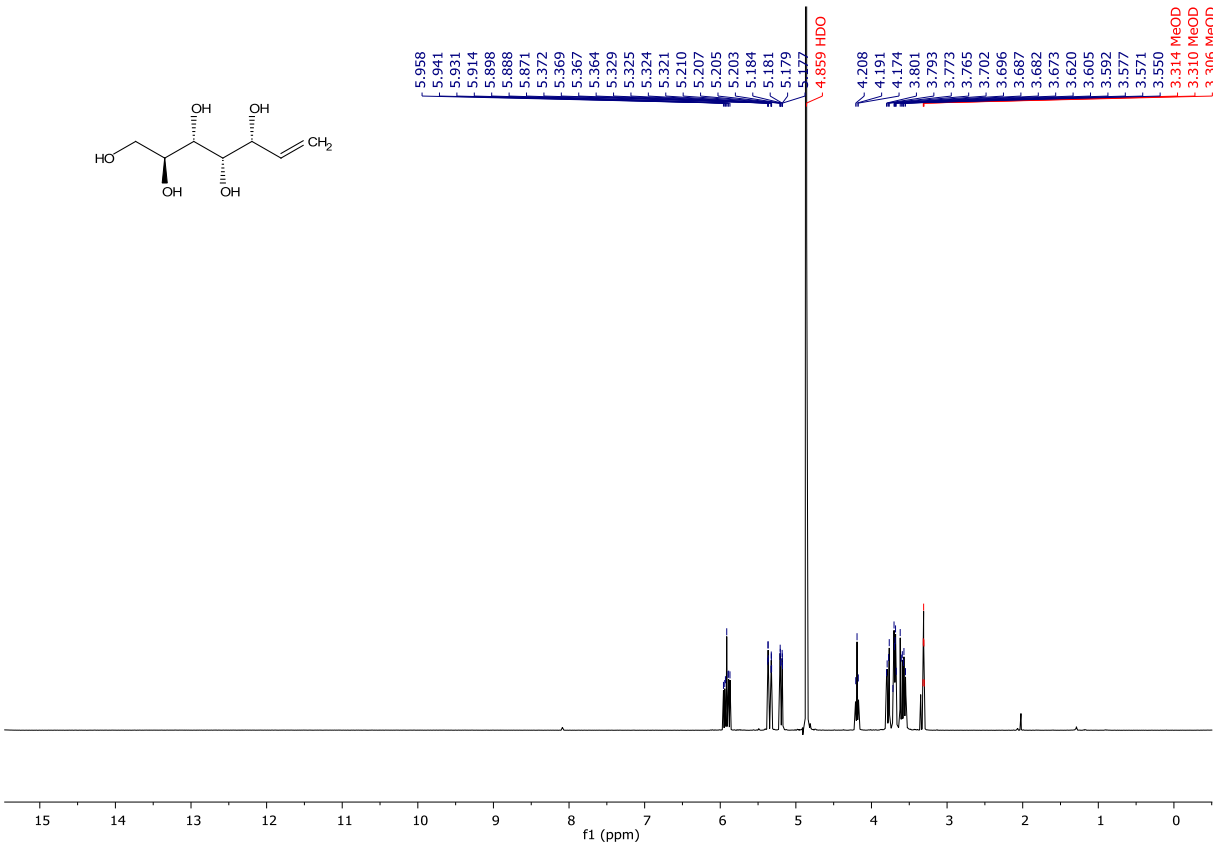

Figure S16. ^{13}C-NMR (101 MHz, MeOD) of **8b**

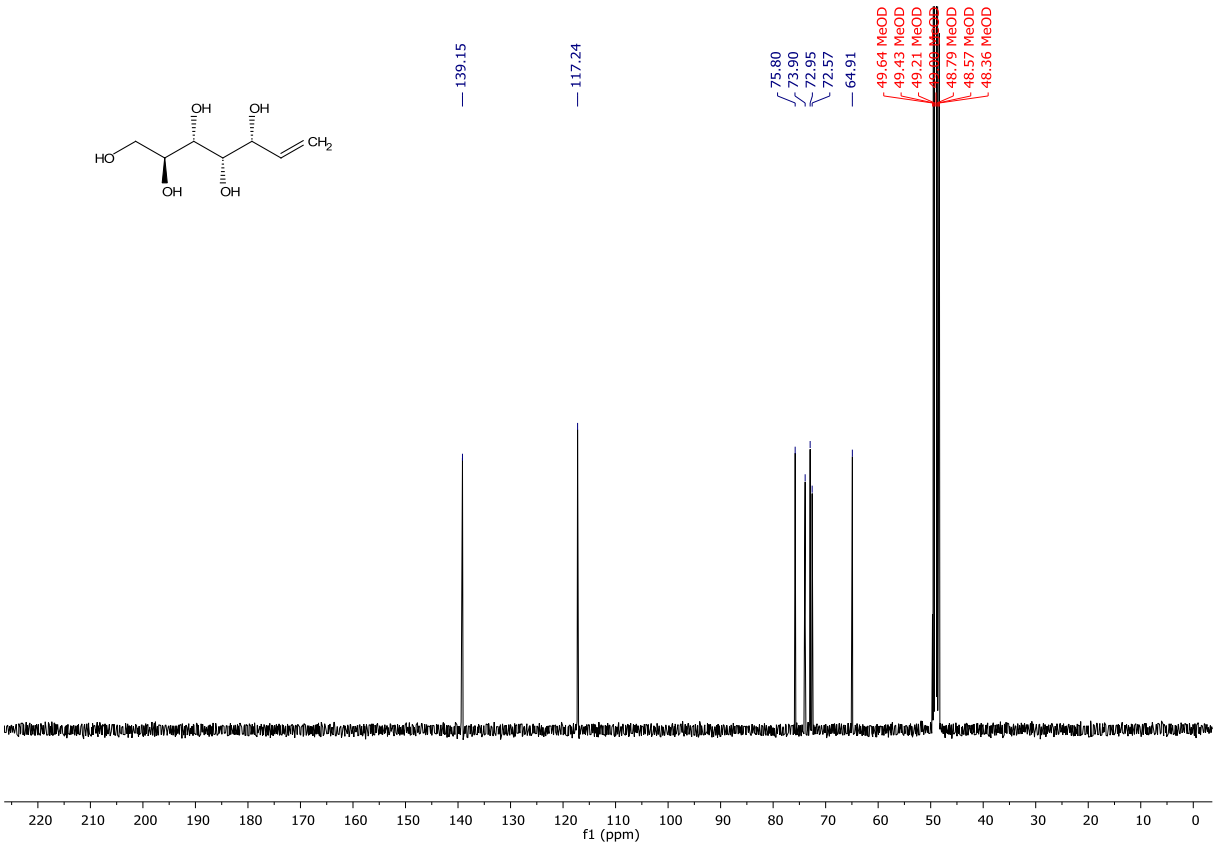

Figure S17. ^{1}H-NMR (400 MHz, MeOD) of **8c** (10% **8d**)

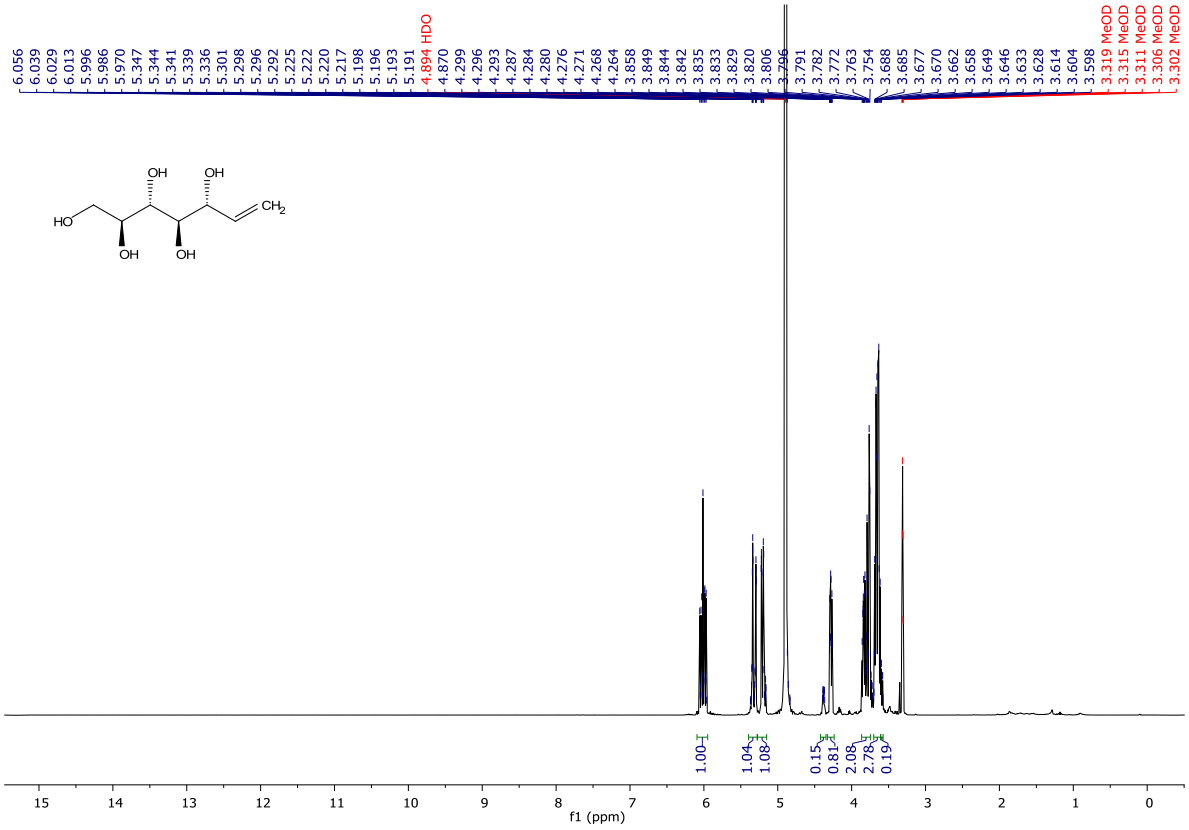

Figure S18. ^{13}C-NMR (101 MHz, MeOD) of **8c** (10% **8d**)

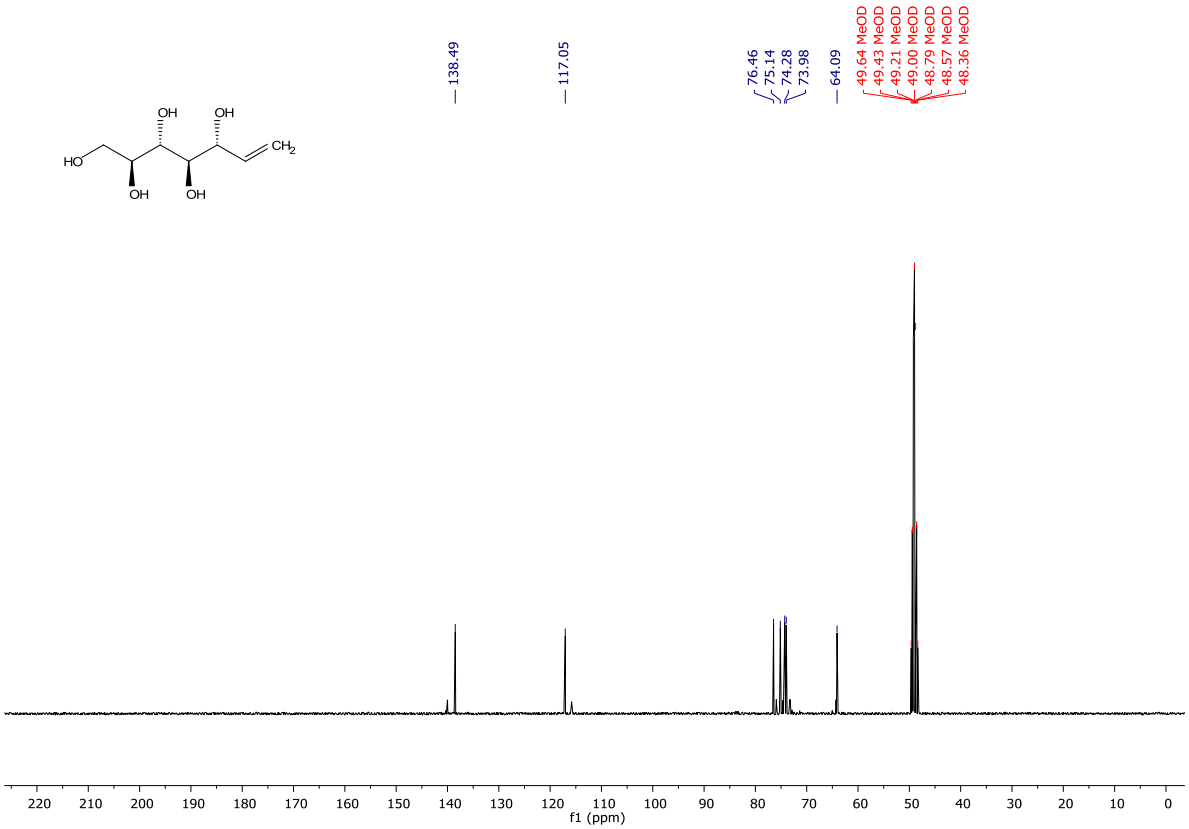

Figure S19. ^{1}H-NMR (400 MHz, $CDCl_3$) of **9a**

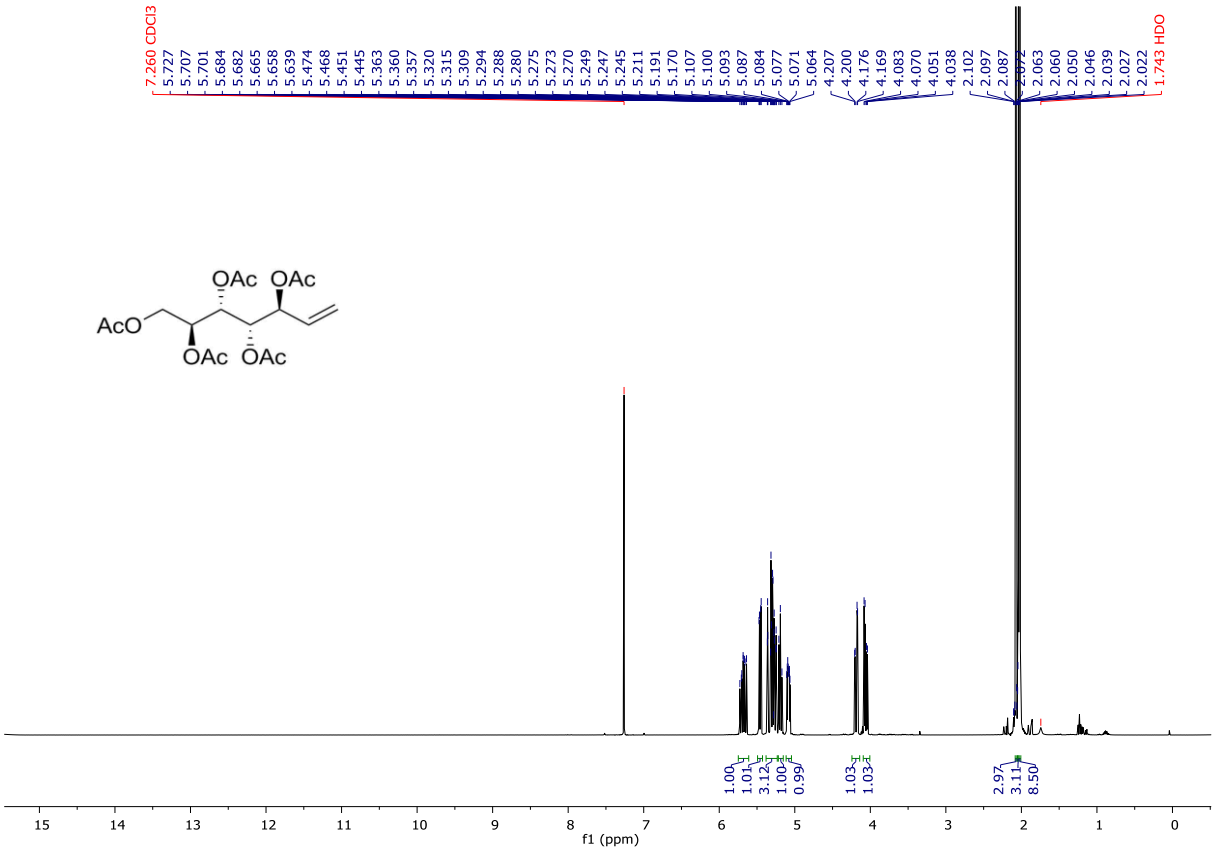

Figure S20. ^{13}C-NMR (101 MHz, $CDCl_3$) of **9a**

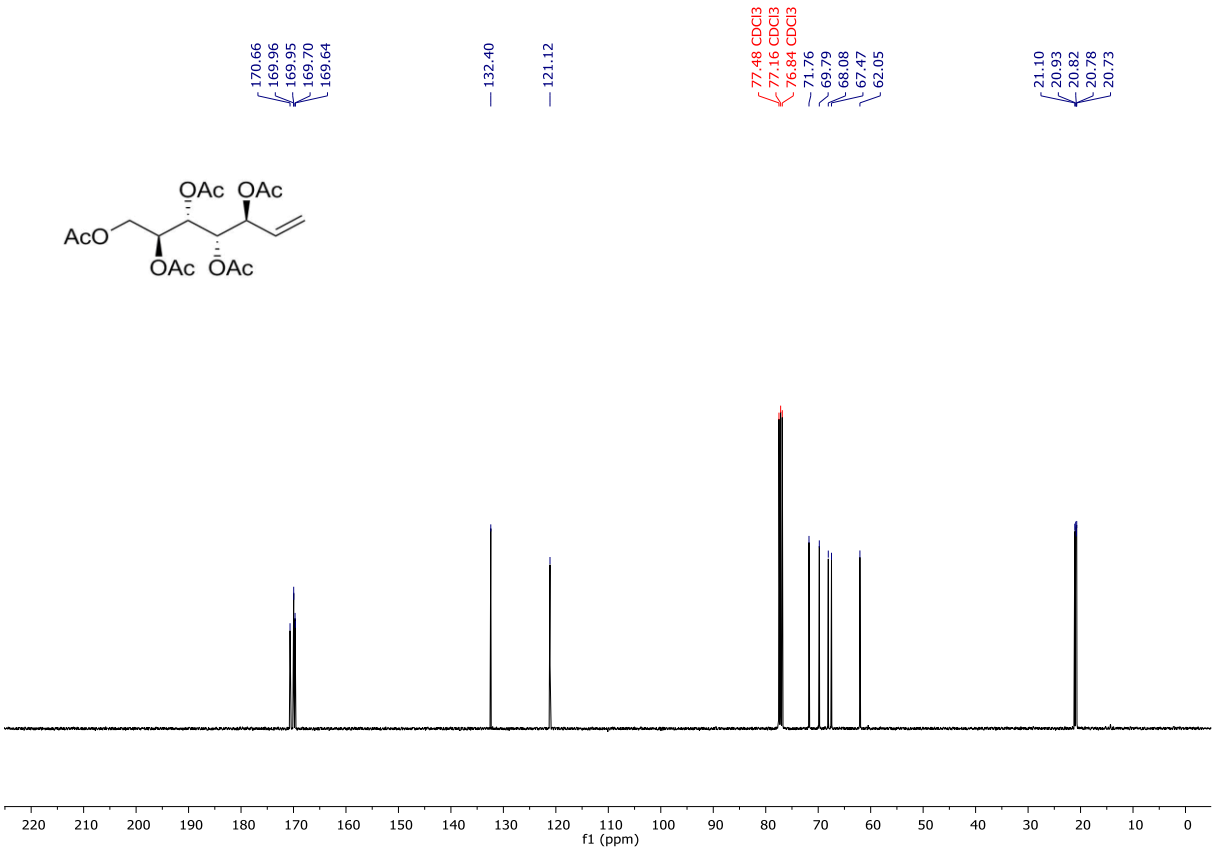

Figure S21. ^{1}H-NMR (400 MHz, $CDCl_3$) of **9b**

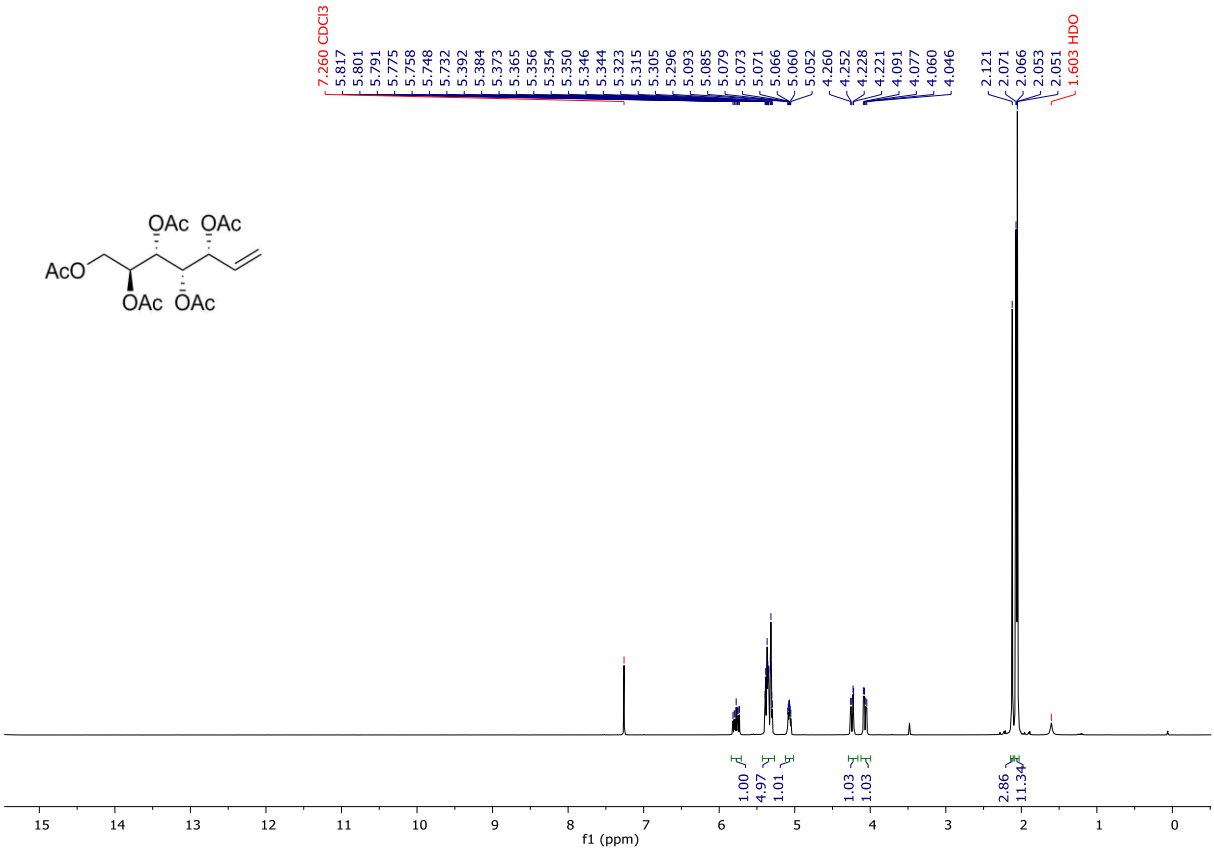

Figure S22. ^{13}C-NMR (101 MHz, $CDCl_3$) of **9b**

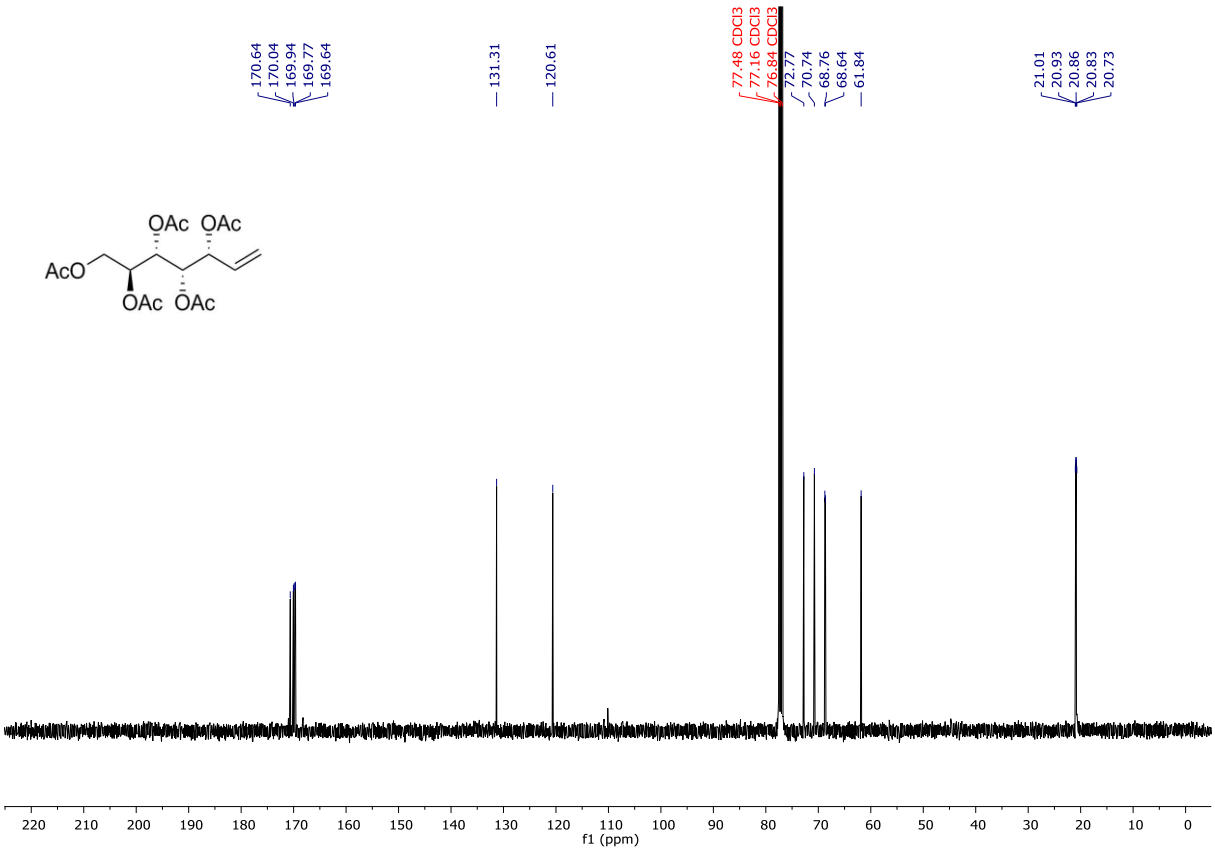

Figure S23. ^{1}H-NMR (400 MHz, CD_2Cl_2) of crude **15**

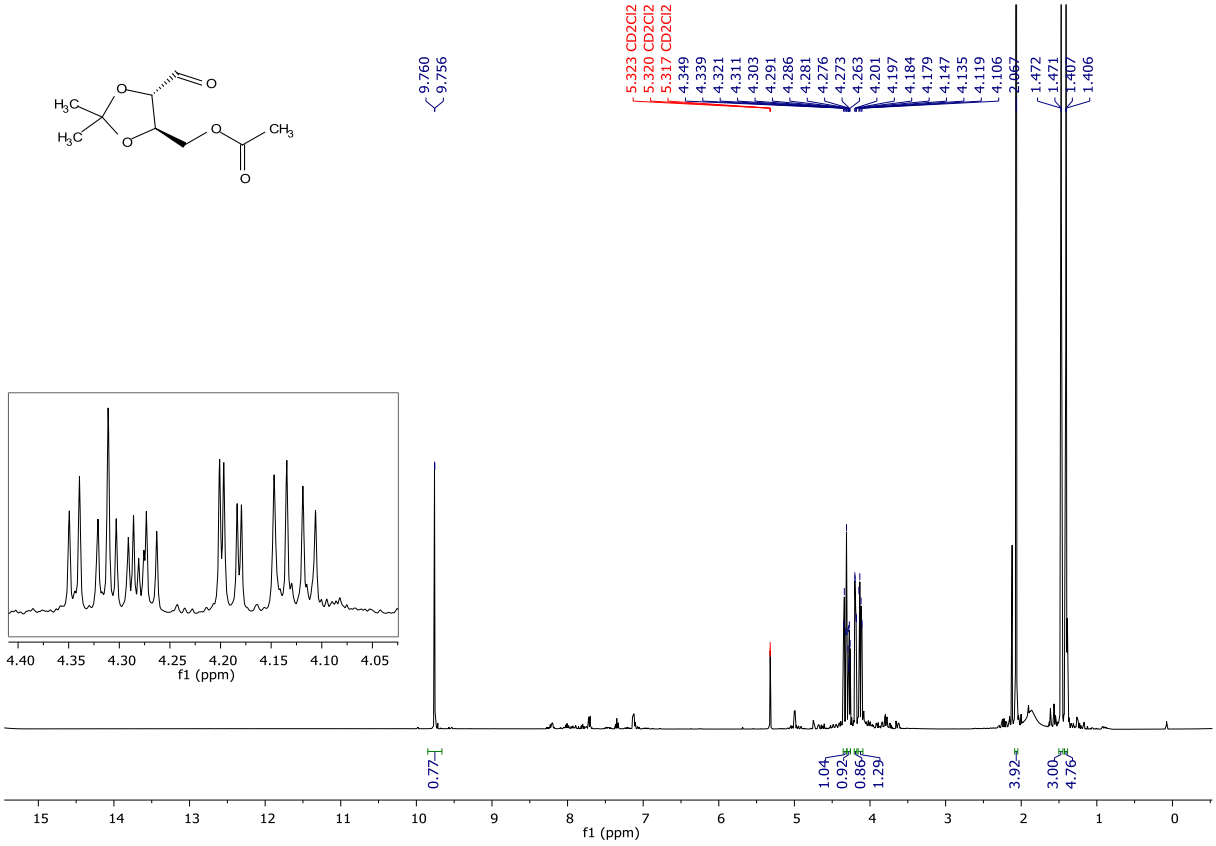

Figure S24. ^{13}C-NMR (101 MHz, CD_2Cl_2) of crude **15**

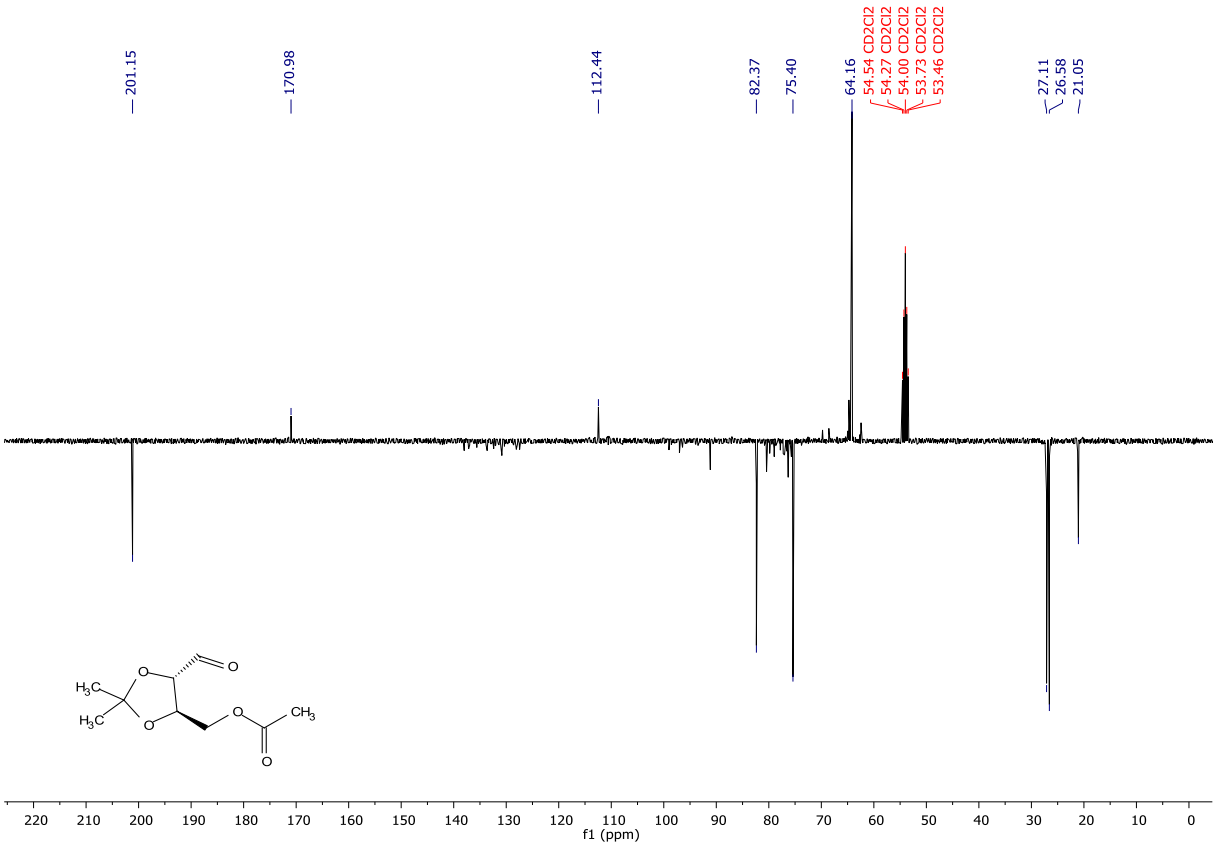

Figure S25. ^{1}H-NMR (400 MHz, MeOD) of **16a** (10% **16c**)

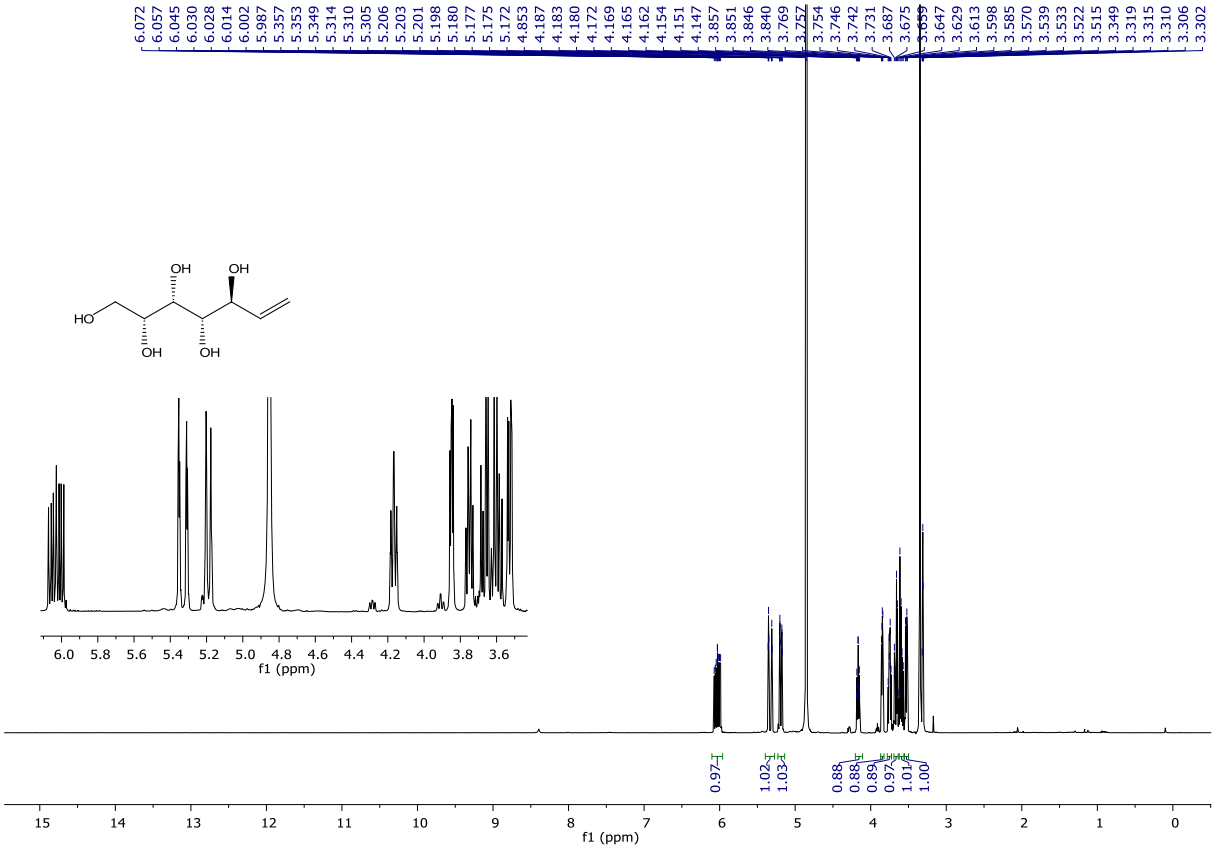

Figure S26. ^{13}C-NMR (101 MHz, MeOD) of **16a** (10% **16c**)

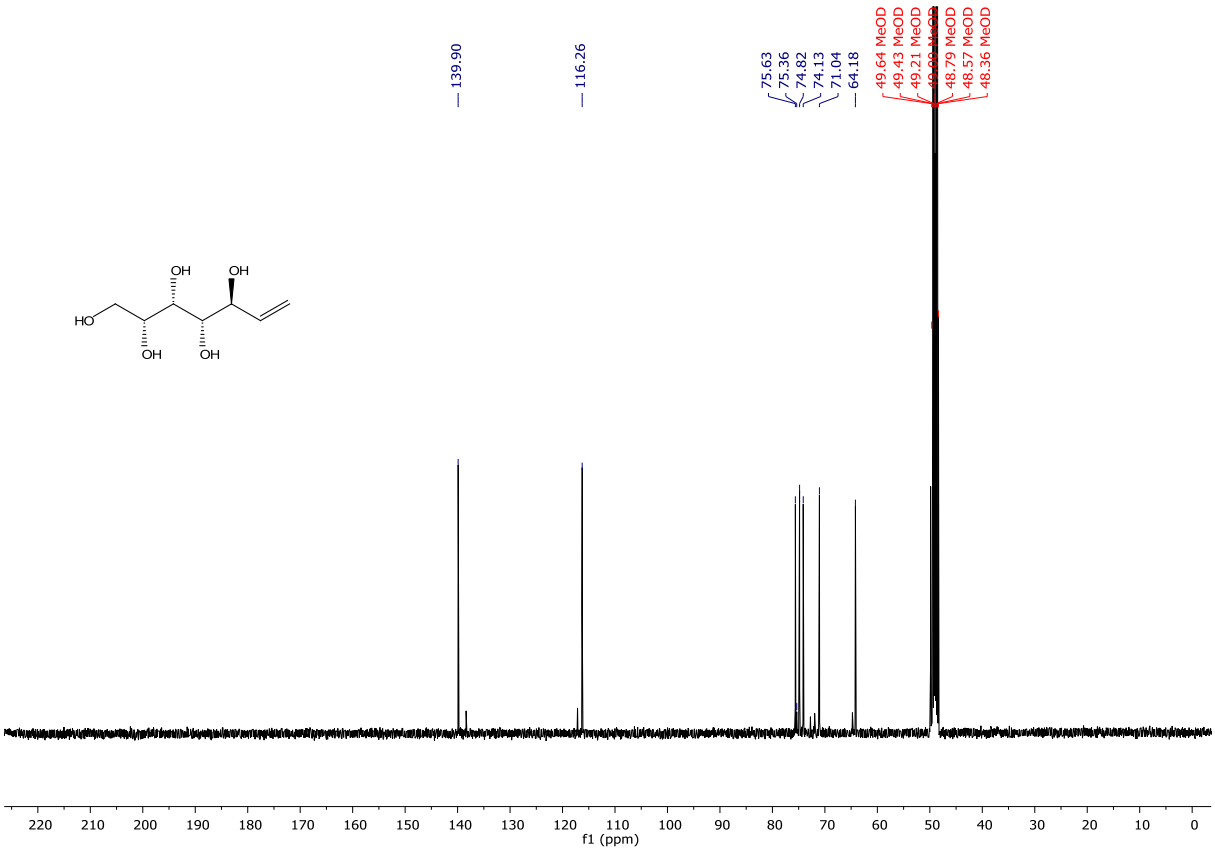

Figure S27. ^{1}H-NMR (400 MHz, MeOD) of **16b**

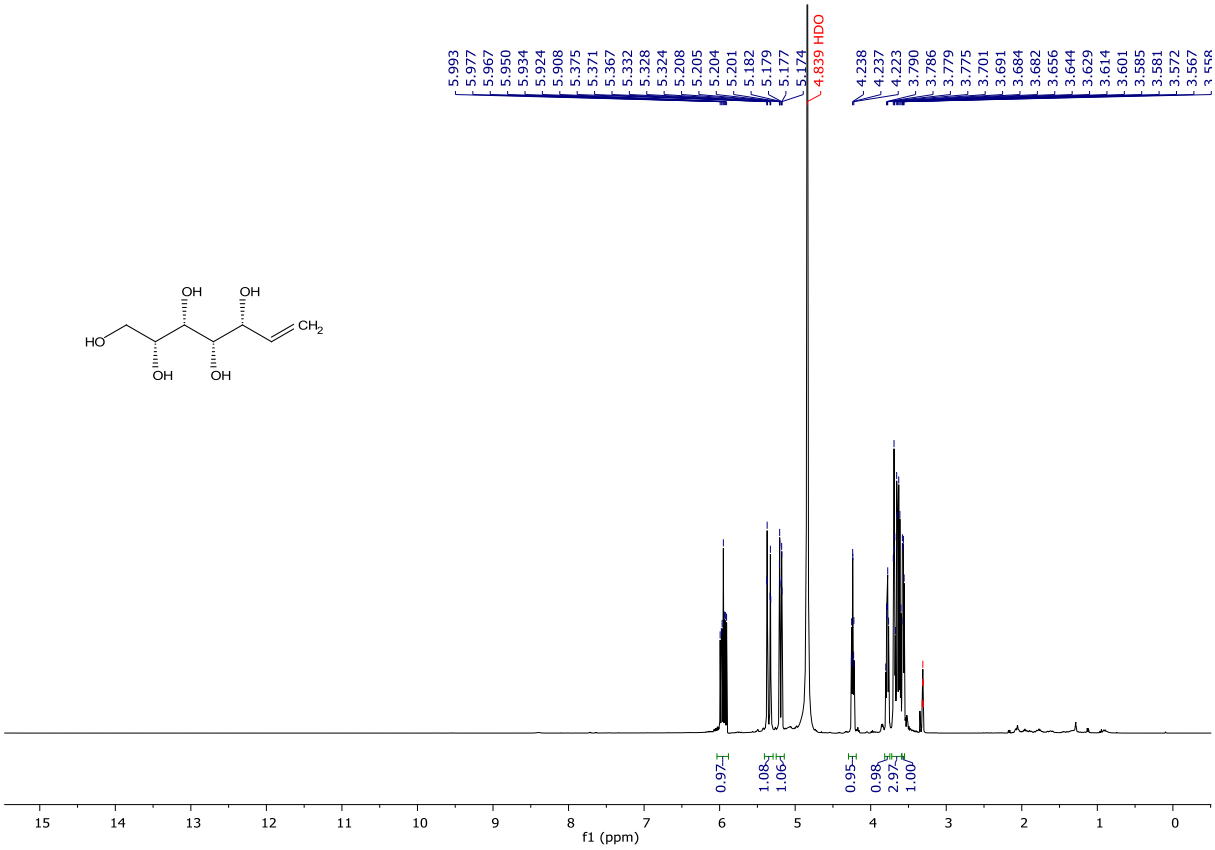

Figure S28. ^{13}C-NMR (101 MHz, MeOD) of **16b**

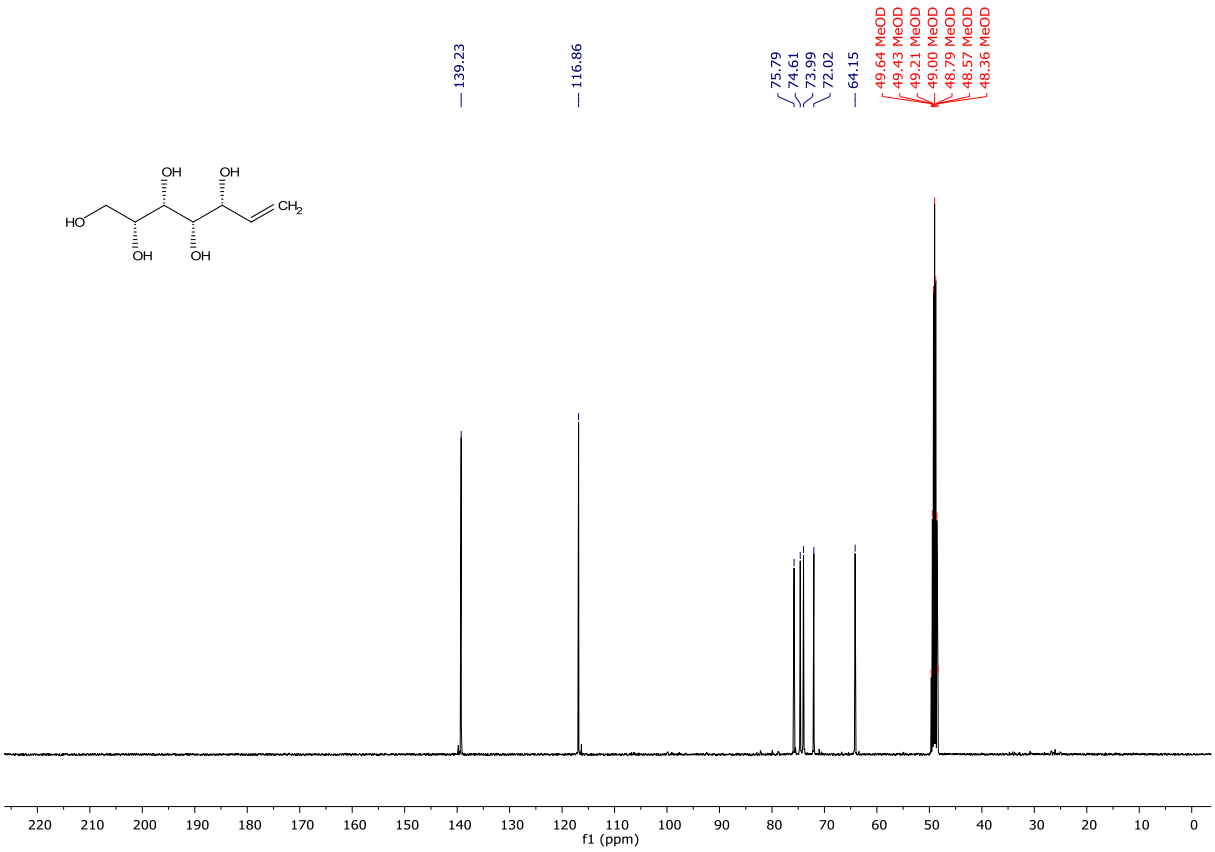

Figure S29 ^{1}H-NMR (400 MHz, MeOD) of **16c**

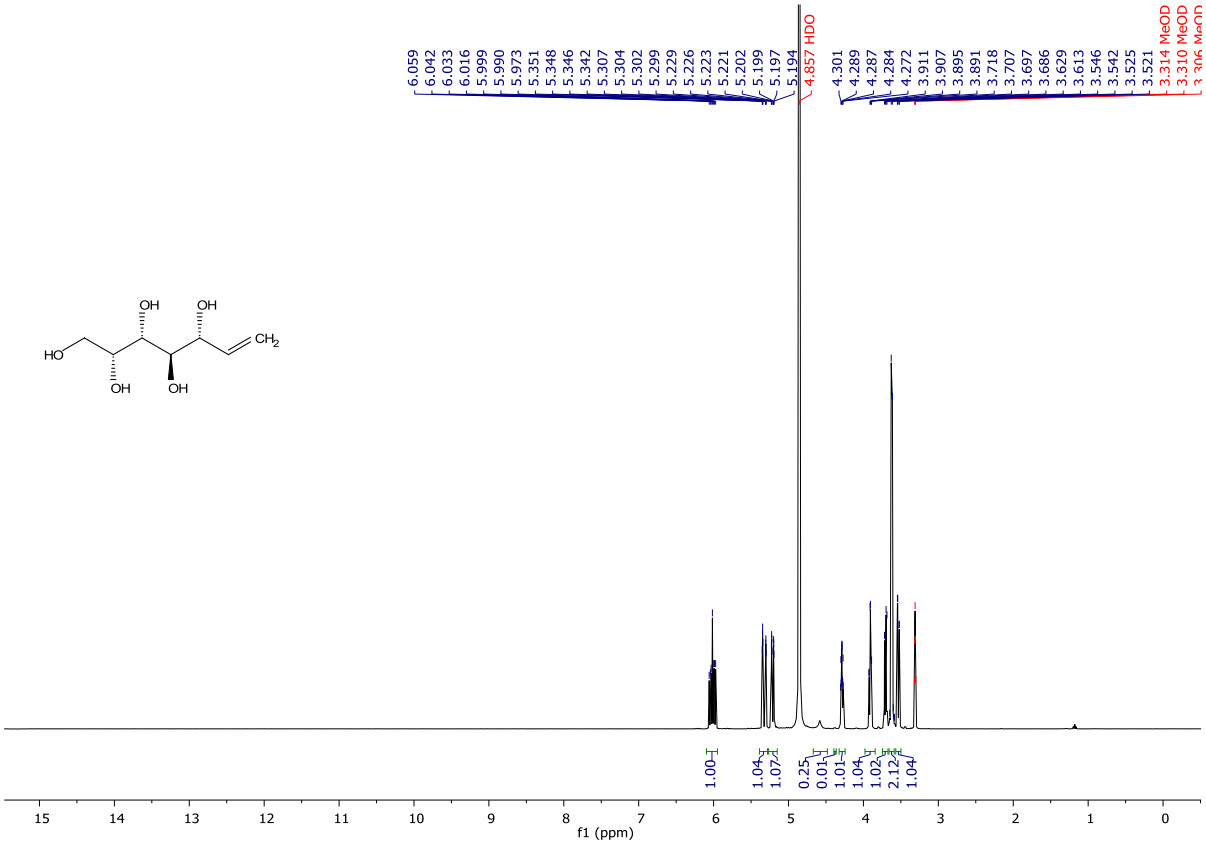

Figure S30. ^{13}C-NMR (101 MHz, MeOD) of **16c**

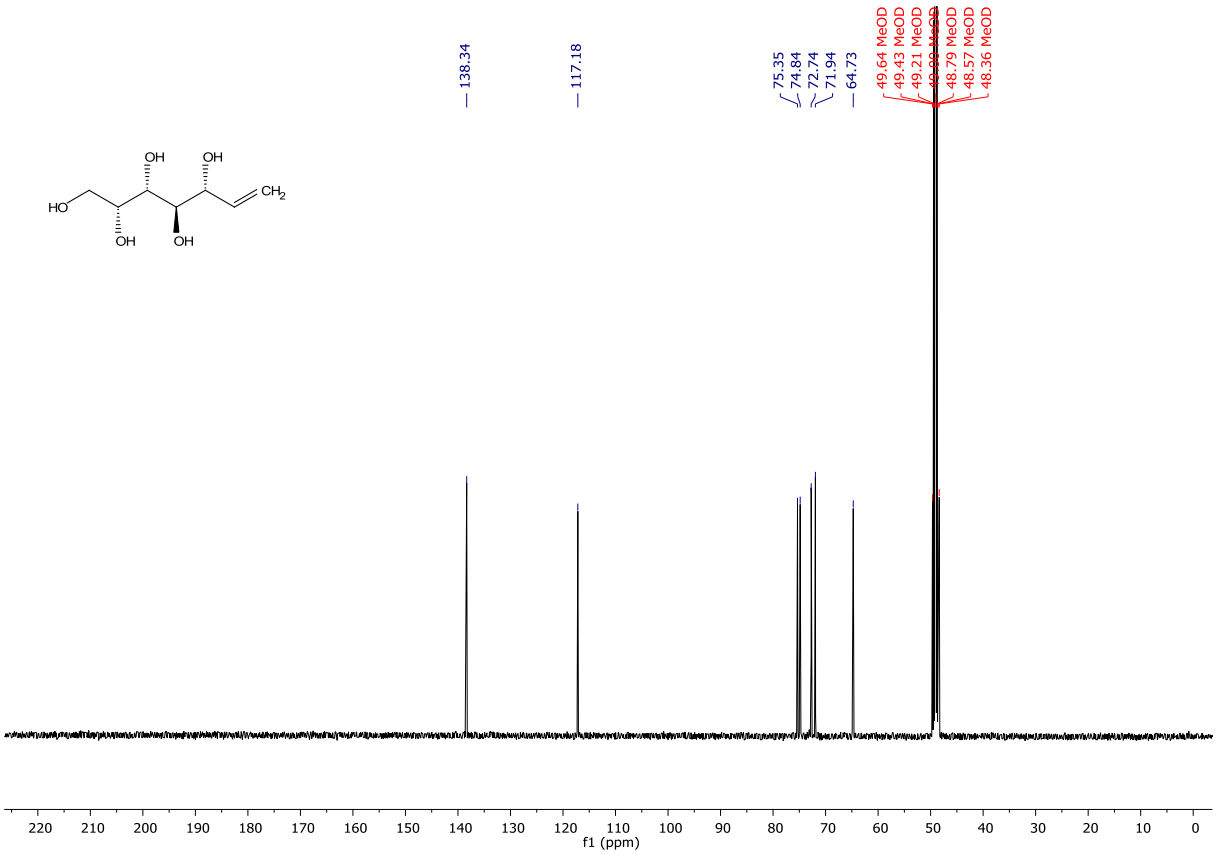

Figure S31. ^{1}H-NMR (400 MHz, MeOD) of **16d** (as minor compound in **16c**)

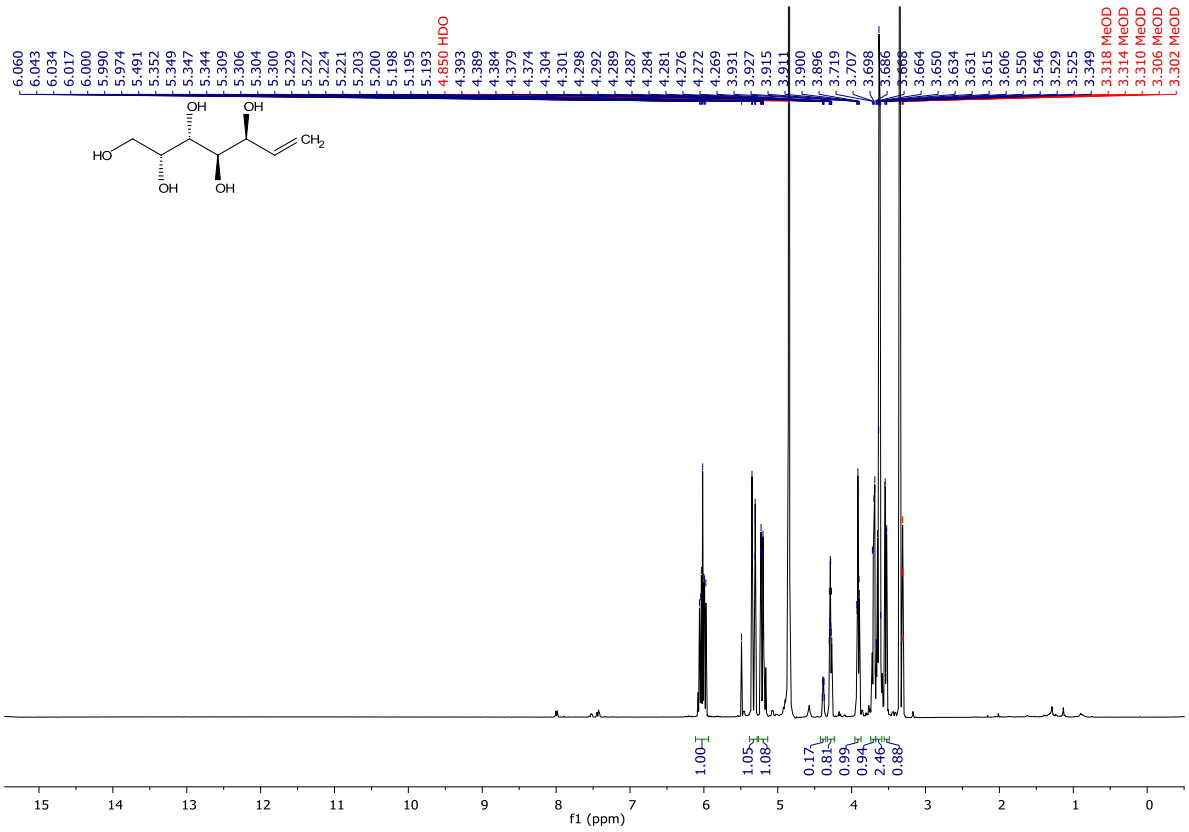

Figure S32. ^{13}C-NMR (101 MHz, MeOD) of **16d** (as minor compound in **16c**)

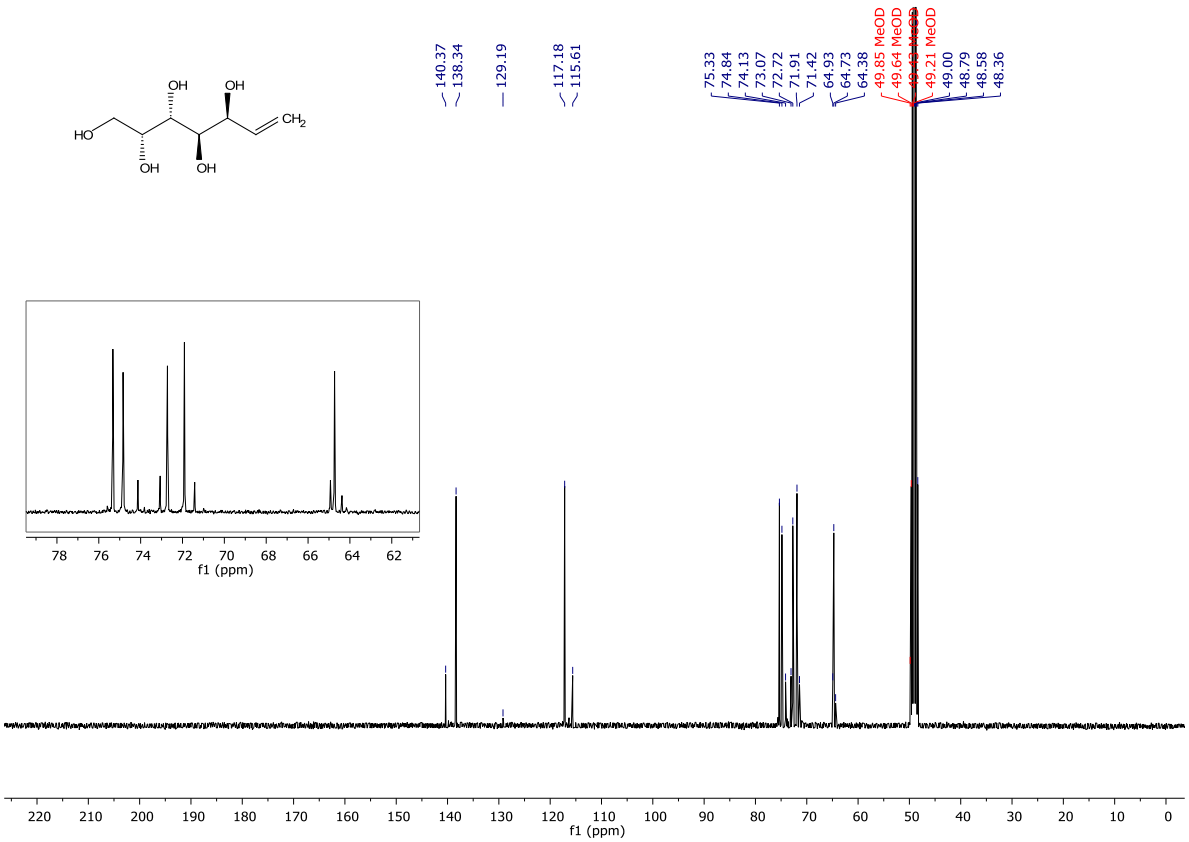

Figure S33. ^{1}H-NMR (400 MHz, $CDCl_3$) of **17a** (10% **17c**)

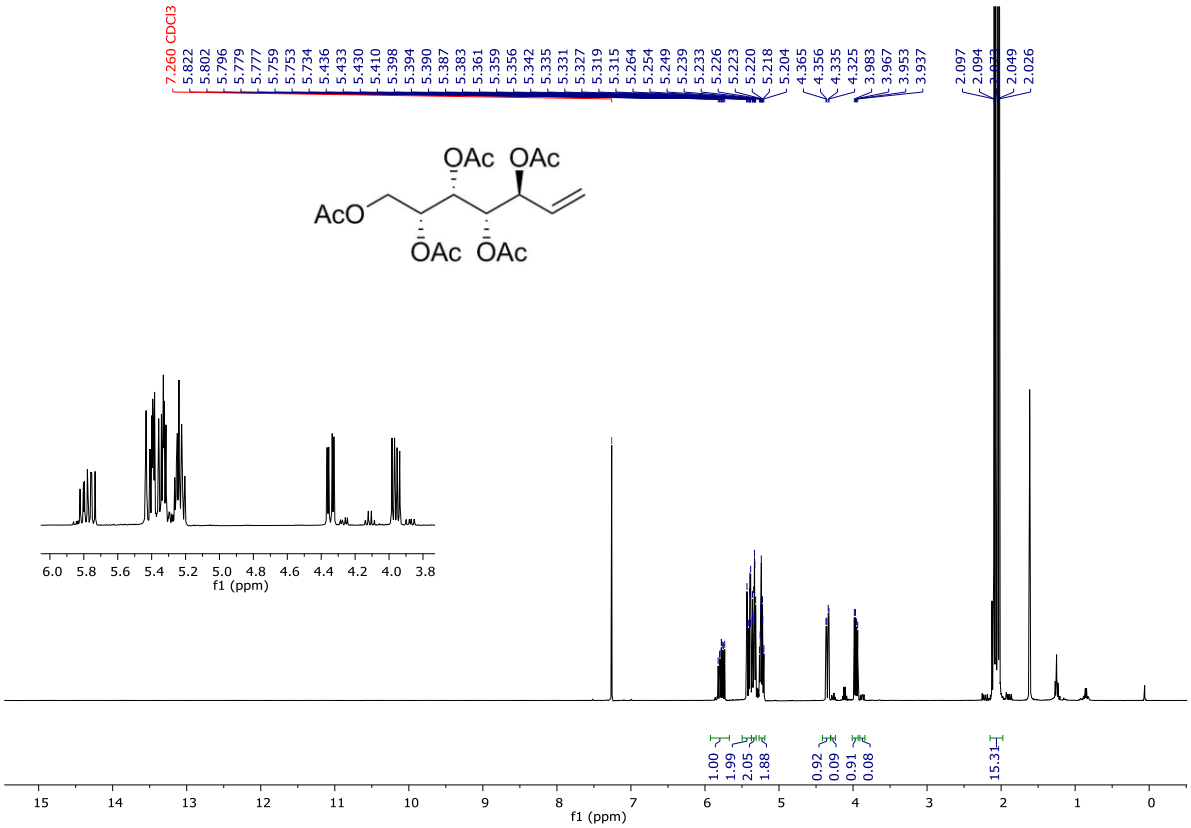

Figure S34. ^{13}C-NMR (101 MHz, $CDCl_3$) of **17a** (10% **17c**)

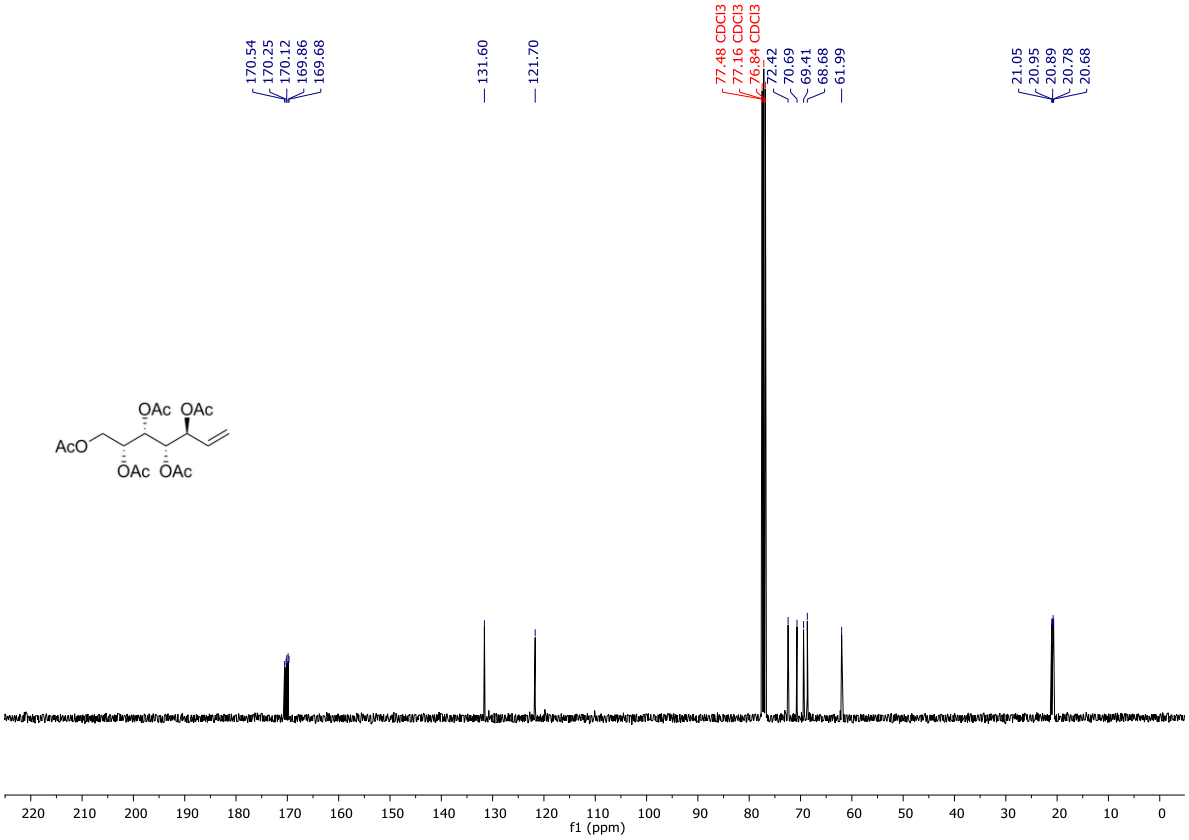

Figure S35. ^{1}H-NMR (400 MHz, $CDCl_3$) of **17b**

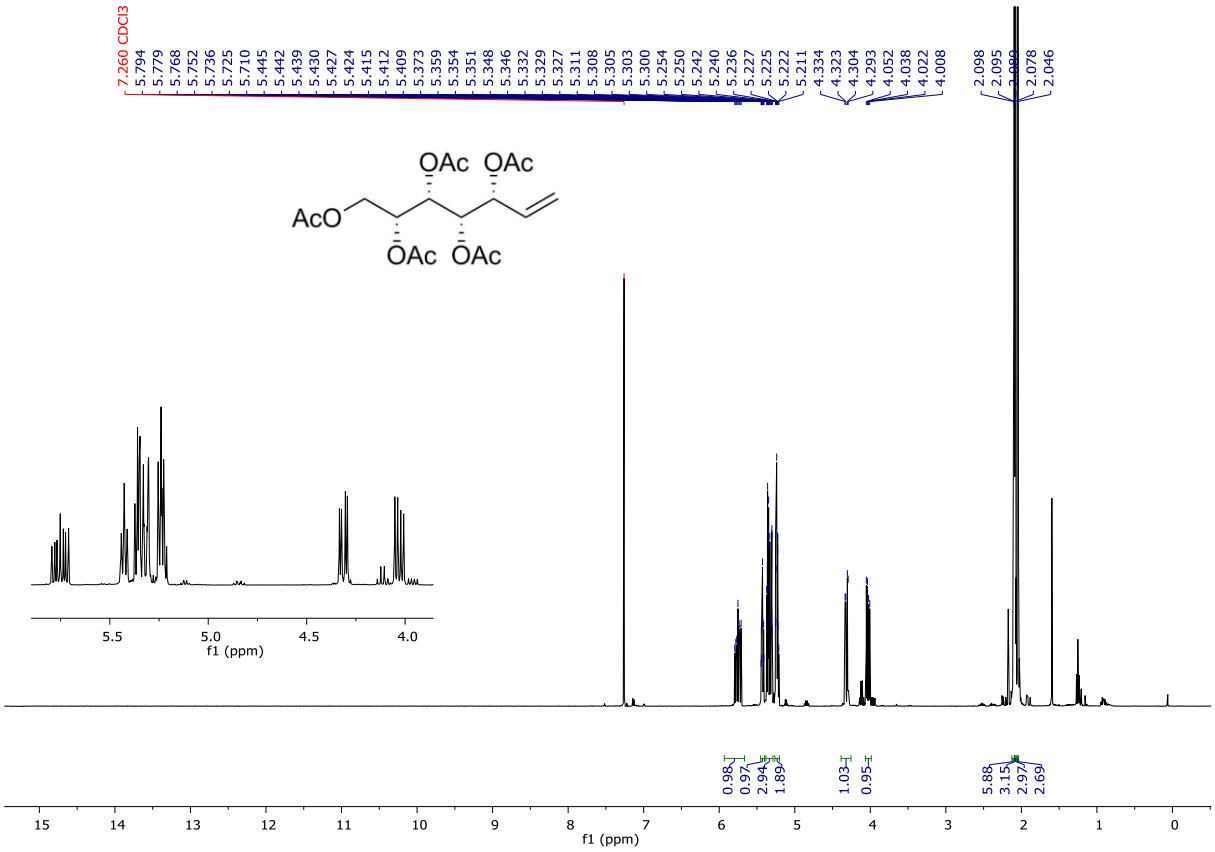

Figure S36. ^{13}C-NMR (101 MHz, $CDCl_3$) of **17b**

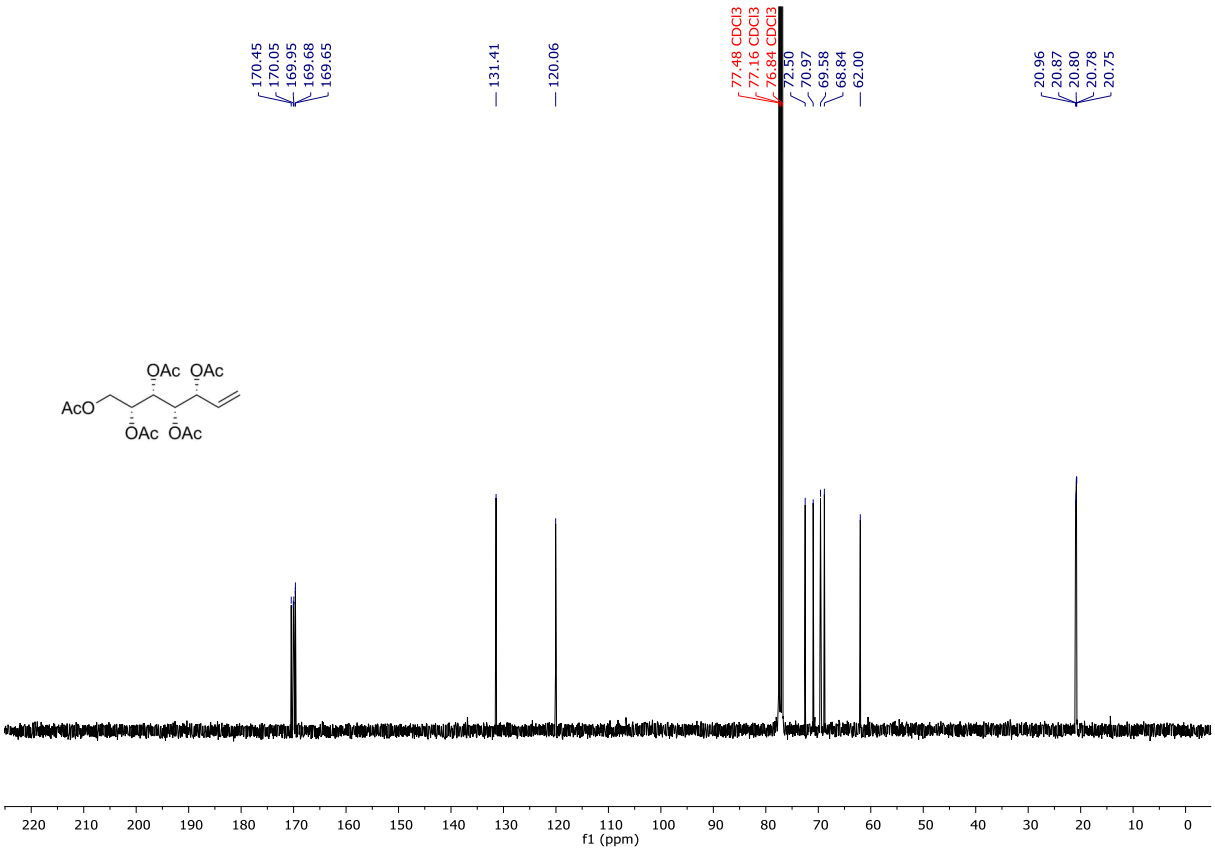

Figure S37. ^{1}H-NMR (400 MHz, $CDCl_3$) of crude **22**

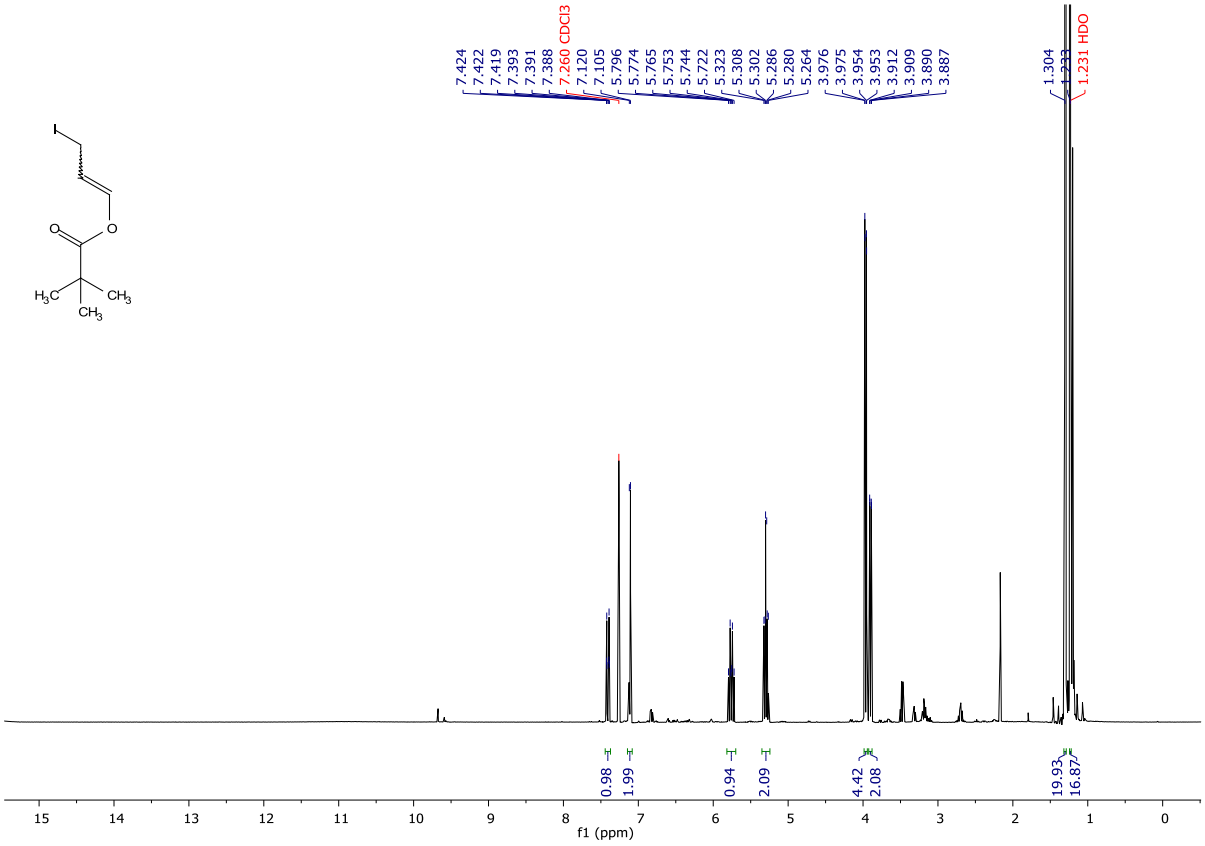

Figure S38. ^{13}C-NMR (101 MHz, $CDCl_3$) of crude **22**

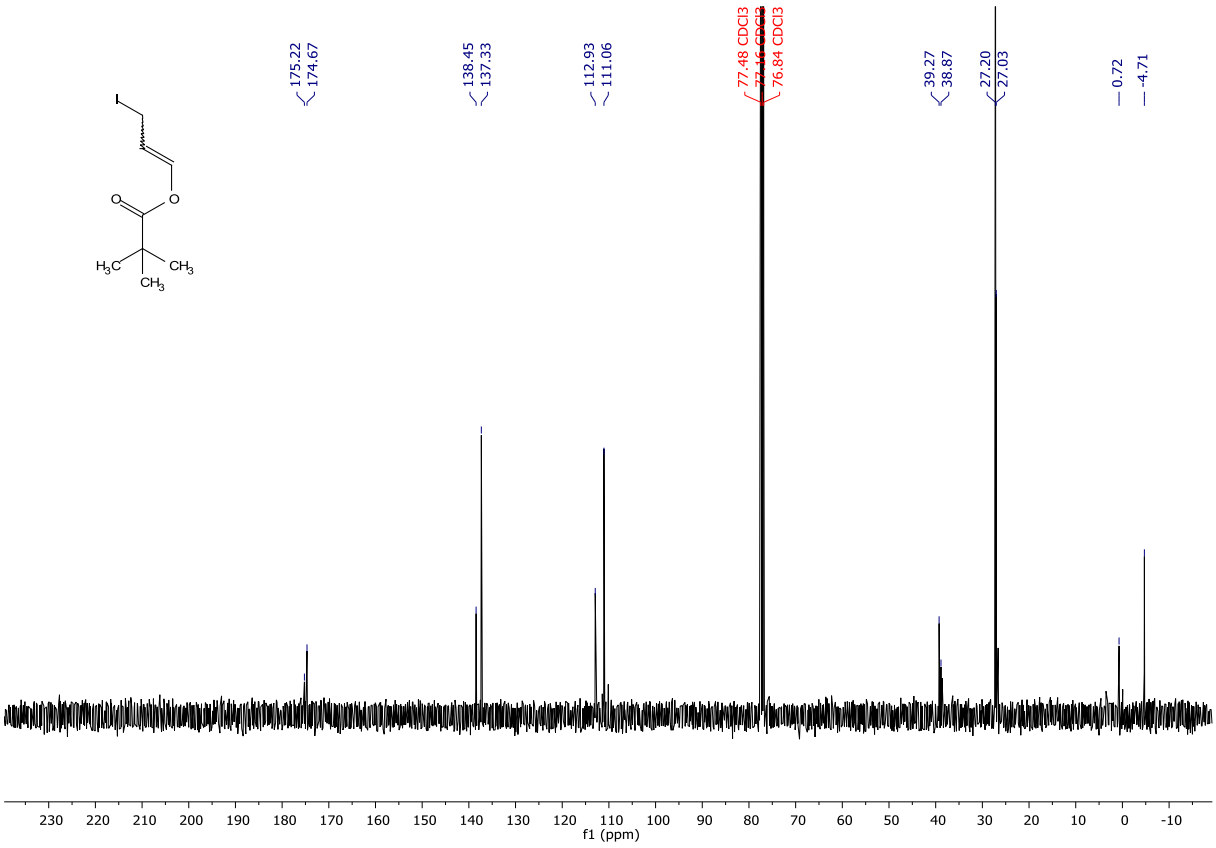

<u>Comparision of the hexoses synthesized *via* acyloxyallylation with commercial authentic samples</u>

Figure S39. Comparison of ^{1}H-NMR of synthesized l-mannose **10** (top) and a commercially available D-mannose (bottom)

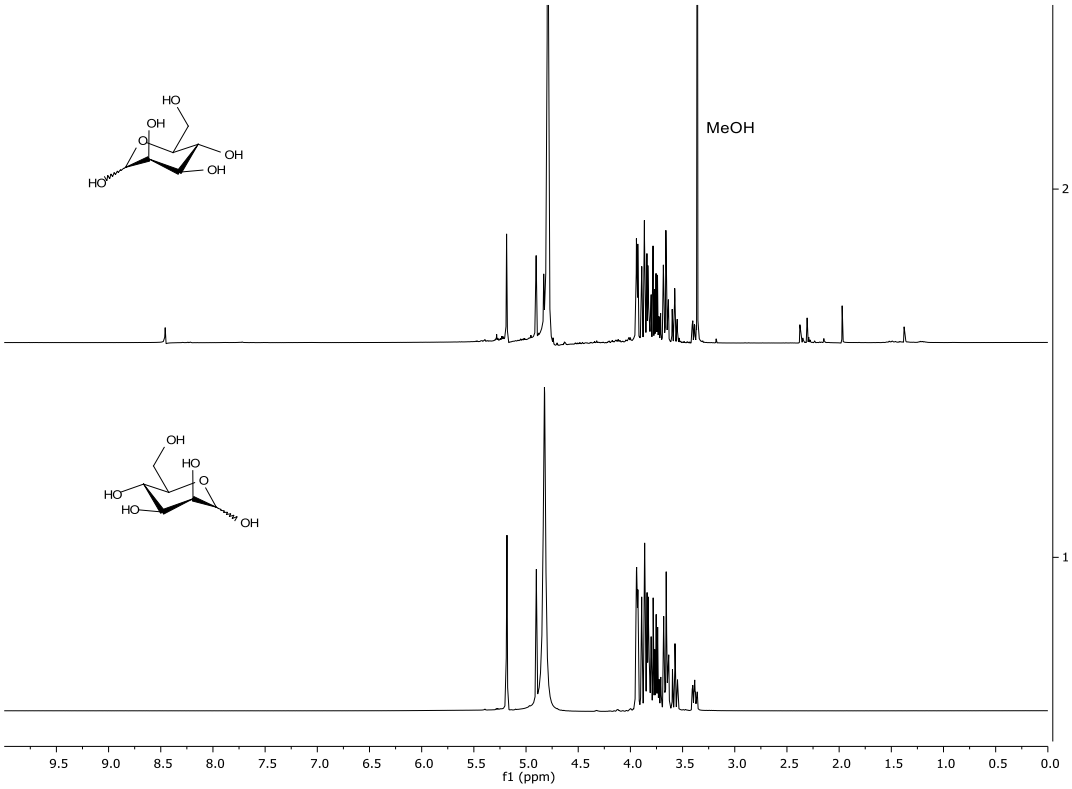

Figure S40. Comparison of ^{13}C-NMR of synthesized L-mannose **10** (top) and a commercially available D-mannose (bottom)

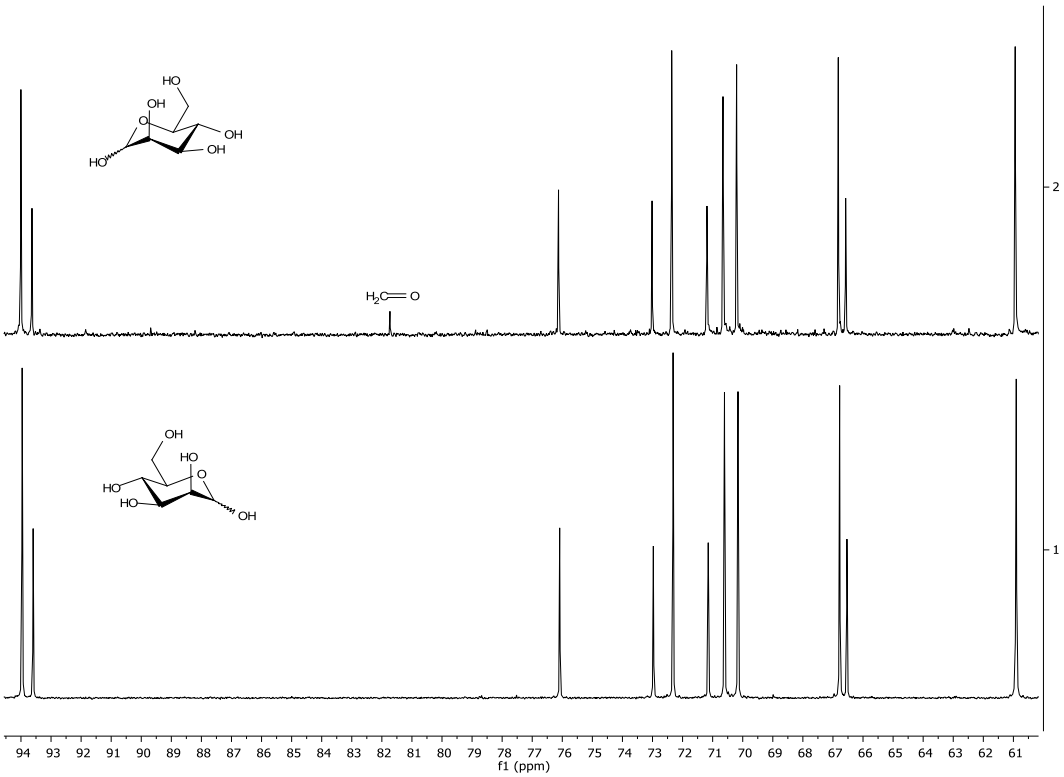

Figure S41. Comparison of ^{1}H-NMR of synthesized L-glucose **11** (above) to commercially available D-glucose (down)

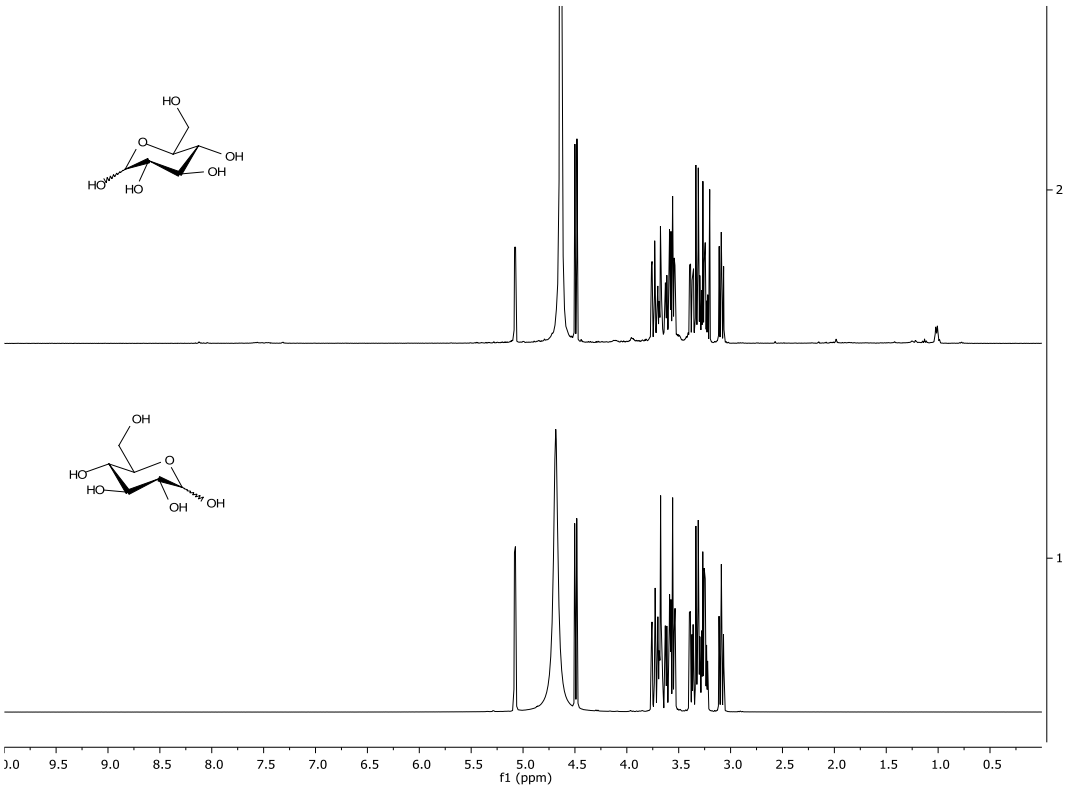

Figure S42. Comparison of ^{13}C-NMR of synthesized L-glucose **11** (above) to commercially available D-glucose (down)

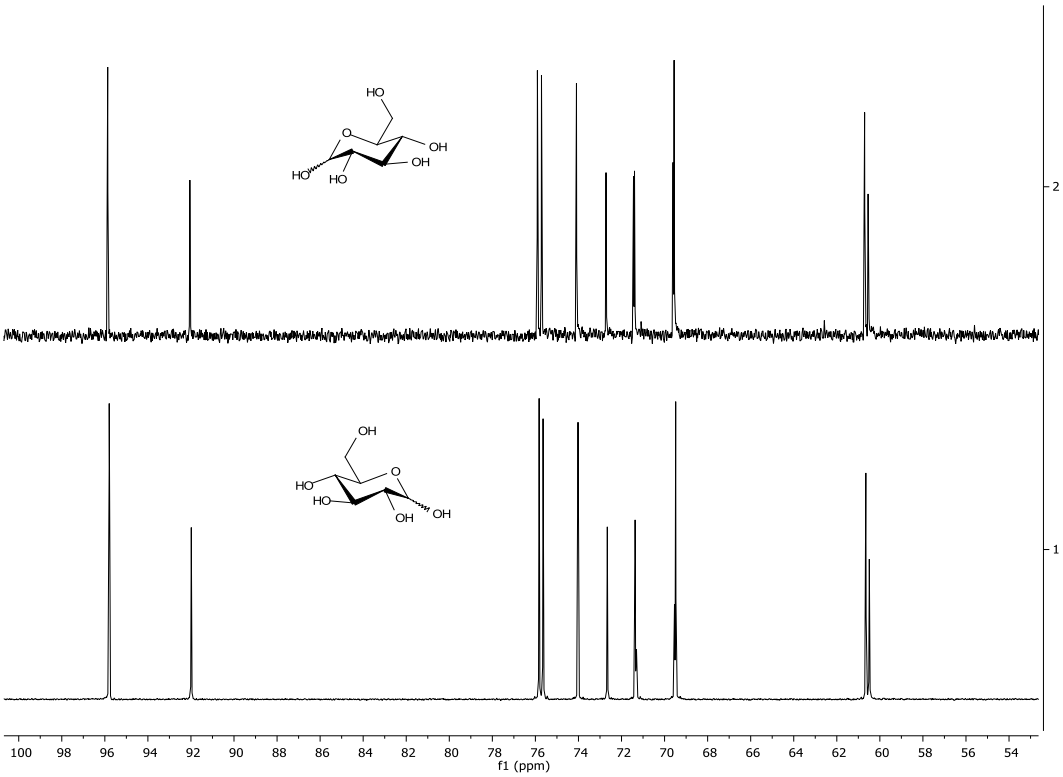

Figure S43. Comparison of ^{1}H-NMR of synthesized L-allose **12** (top) and commercial D-allose (bottom)

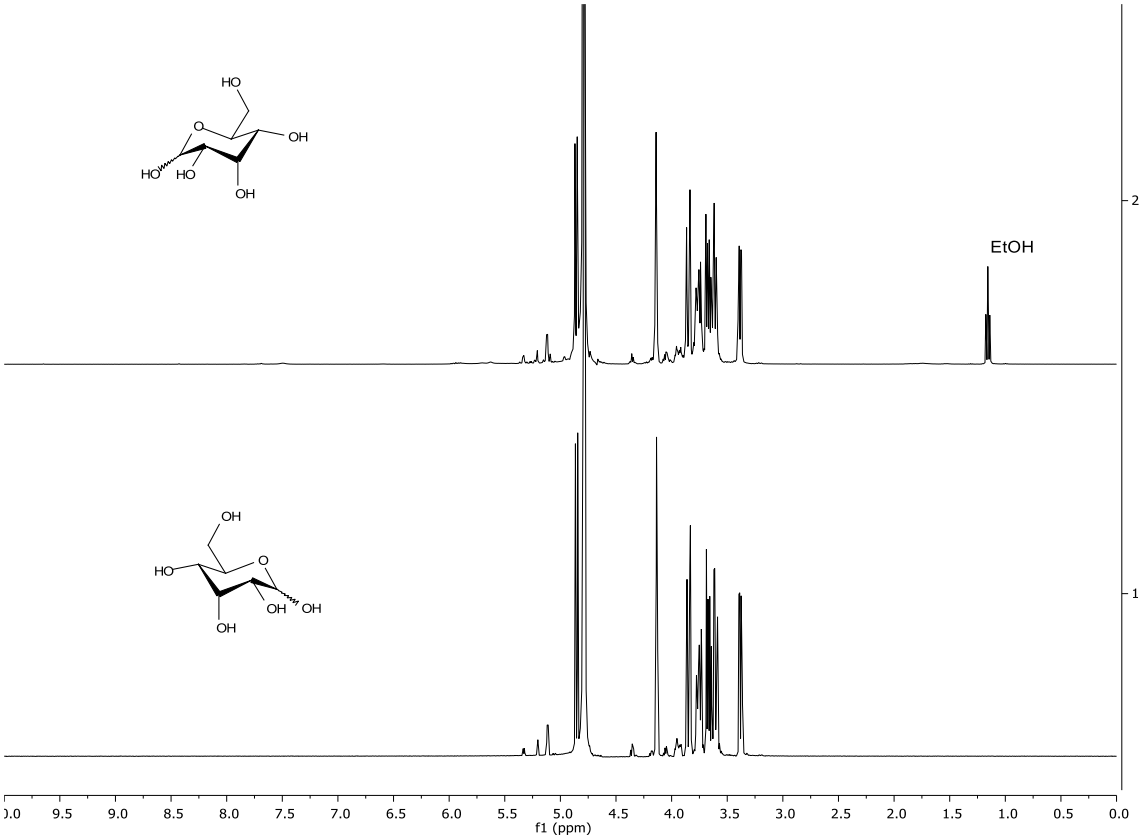

Figure S44. Comparison of ^{13}C-NMR of synthesized L-allose **12** (top, APT) and commercial D-allose (bottom)

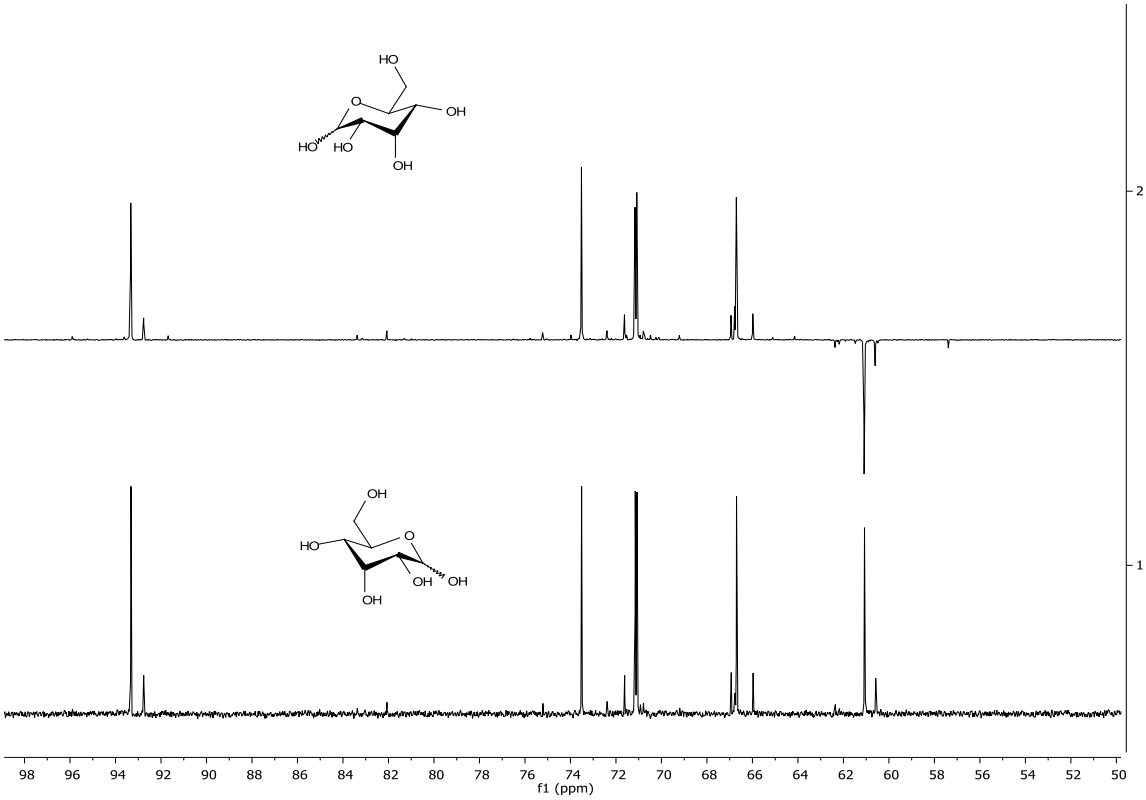

Figure S45. Comparison of ^{1}H-NMR of a synthesized mixture of L-altrose **13** and L-allose **12** (top) and commercial D-altrose (bottom)

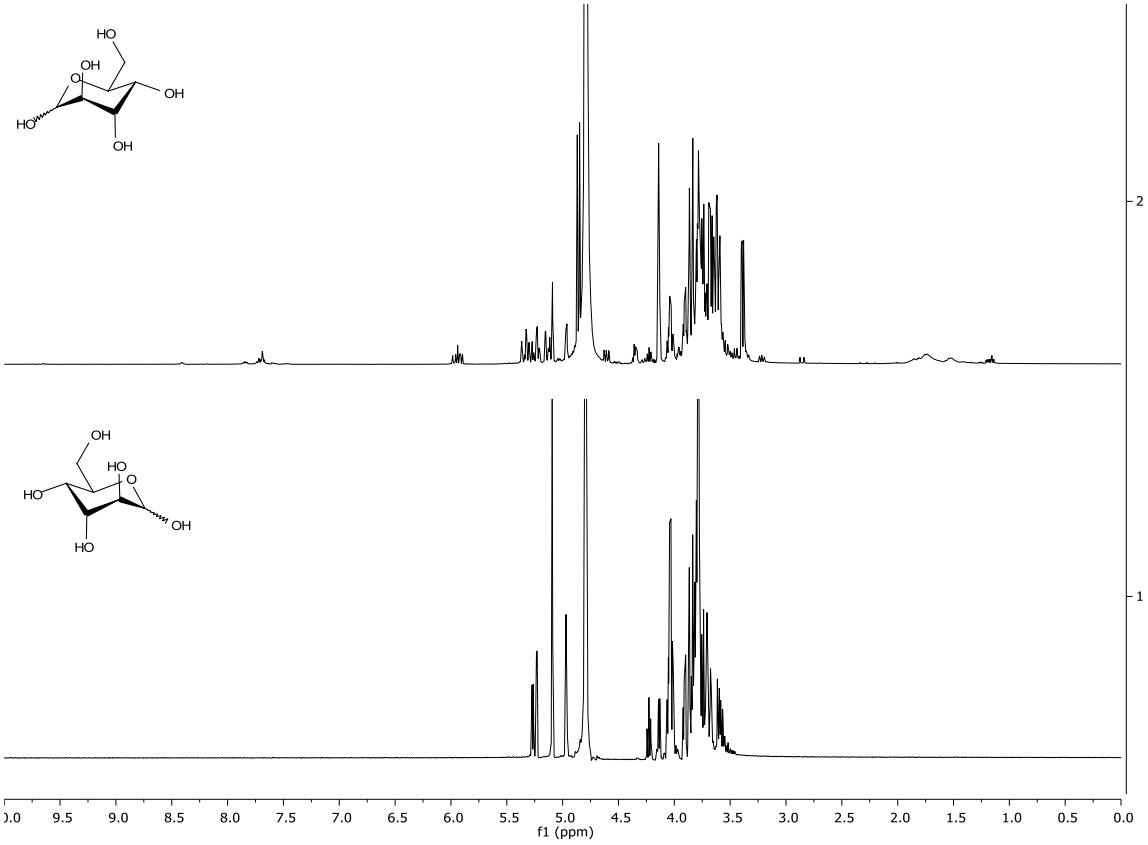

Figure S46. Comparison of ^{13}C-NMR of a synthesized mixture of L-altrose **13** and L-allose **12** (middle) and commercial D-altrose (top) and D-allose (bottom)

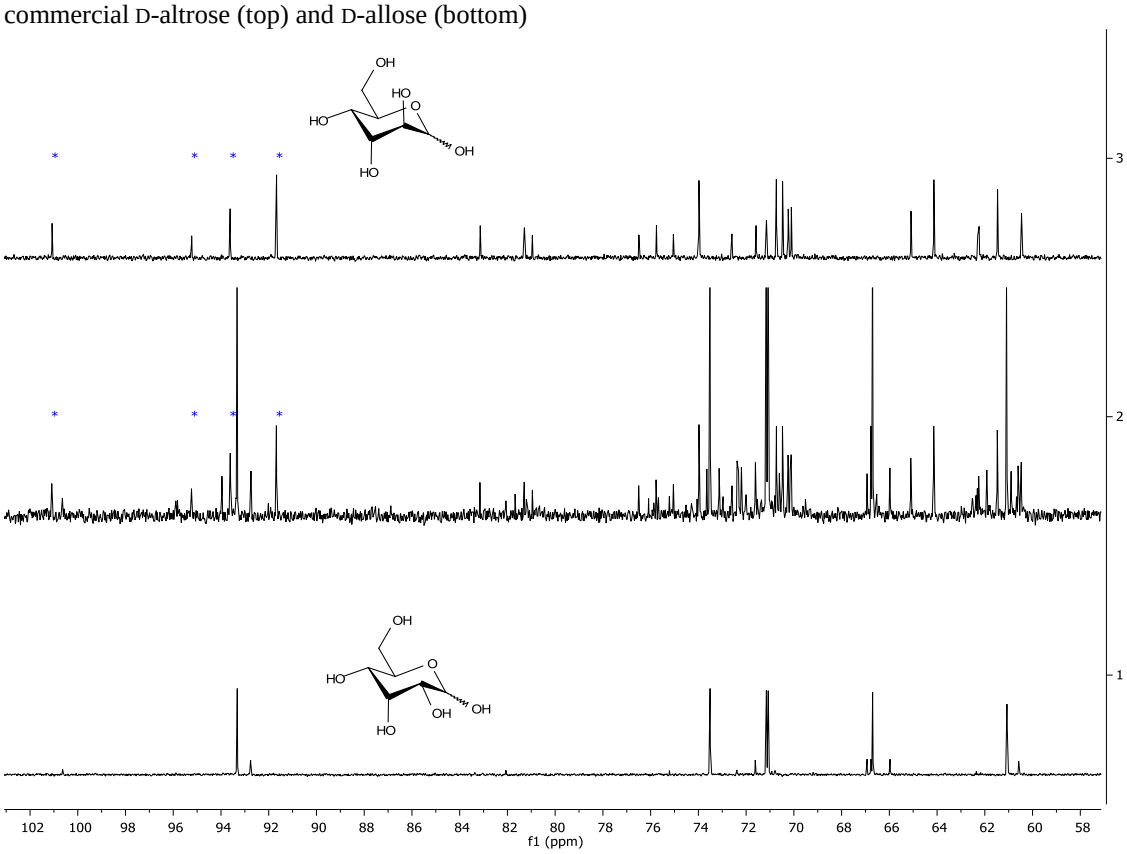

Figure S47. Comparison of ^{1}H-NMR of synthesized (top) and commercially available (bottom) D-gulose **18**

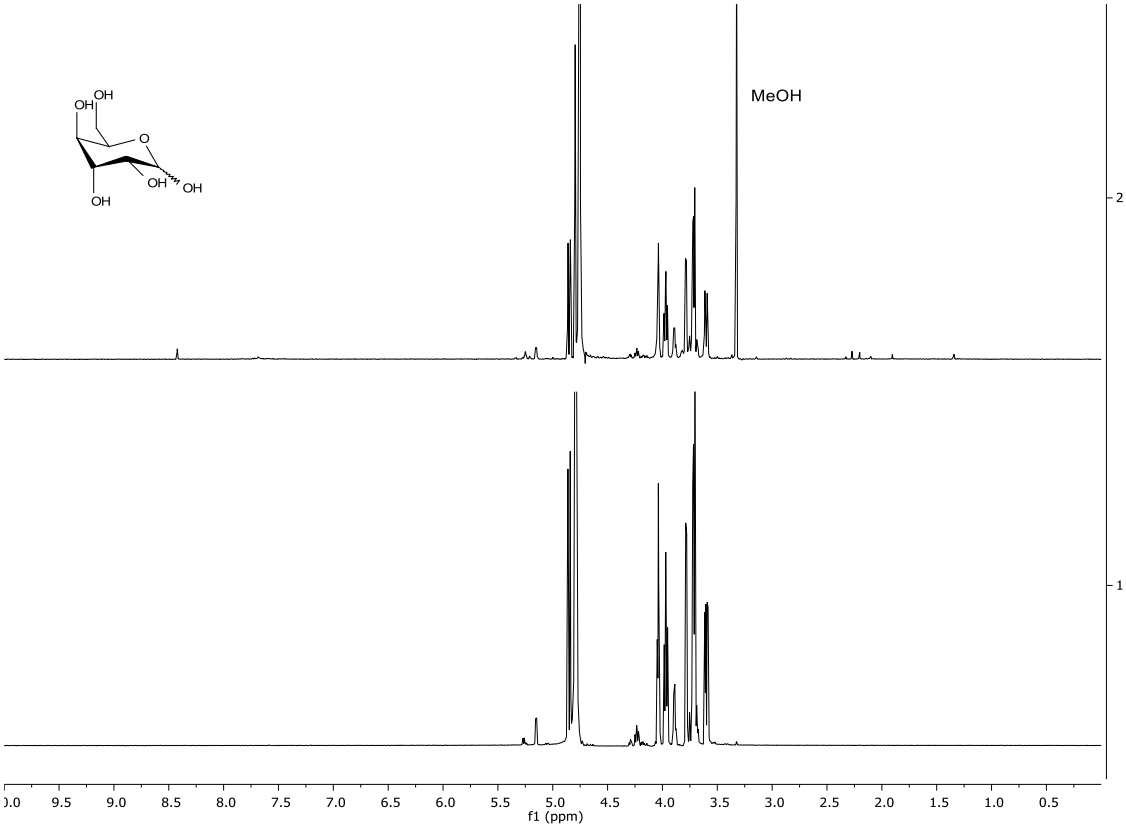

Figure S48. Comparison of ^{13}C-NMR of synthesized (top) and commercially available (bottom) D-gulose **18**

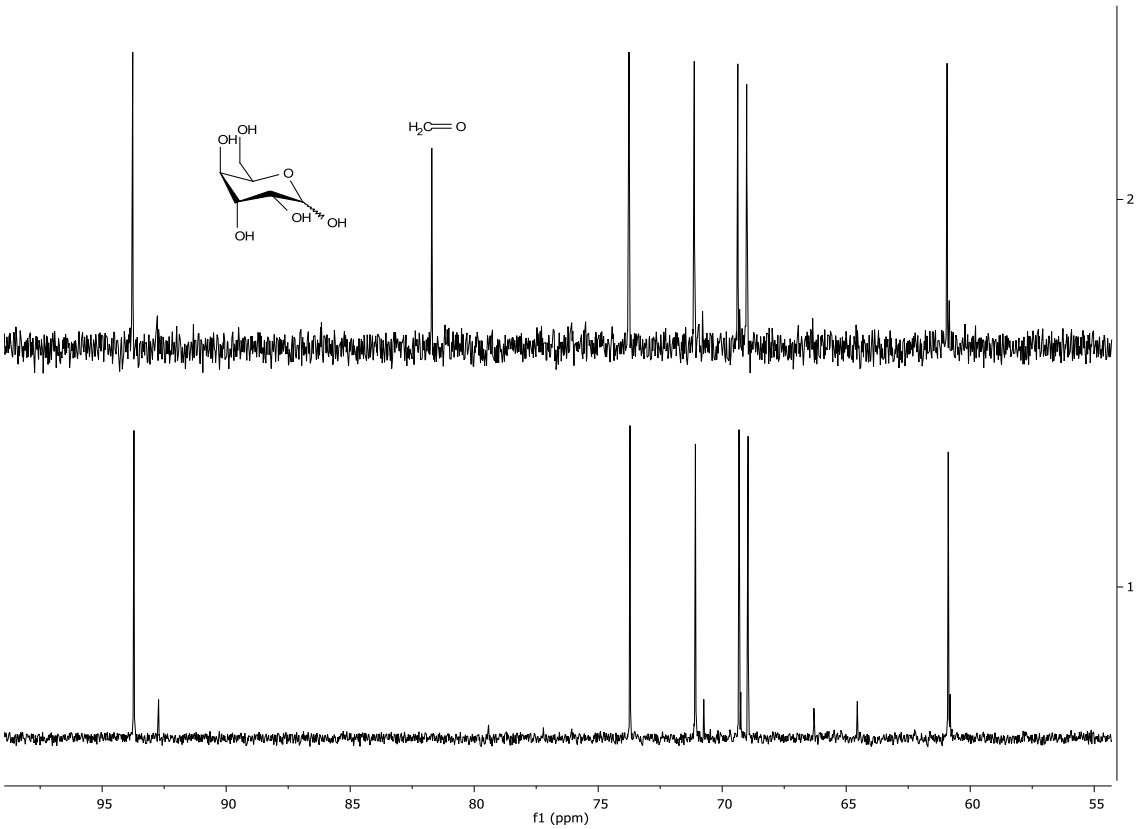

Figure S49. Comparison of ^{1}H-NMR of synthesized (top) and a commercially (bottom) D-idose **19**

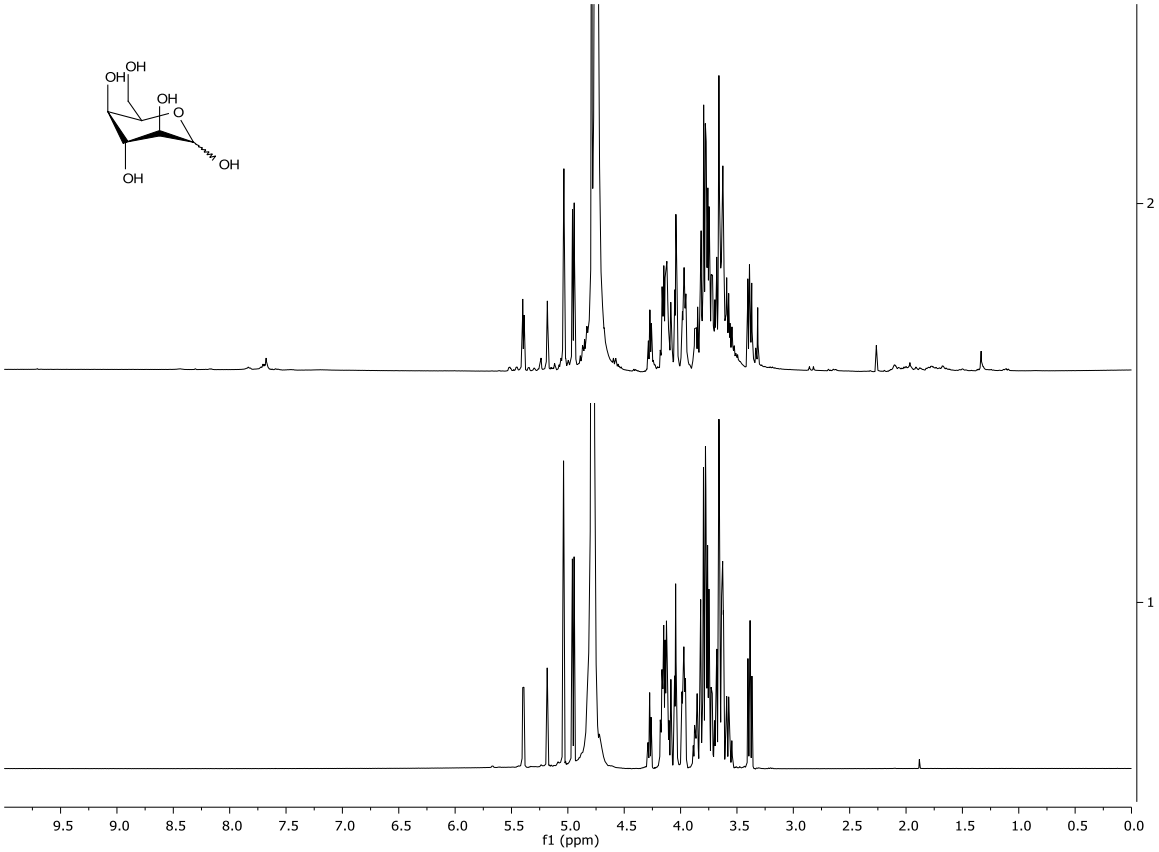

Figure S50. Comparison of ^{13}C-NMR of synthesized (top) and a commercially (bottom) D-idose **19**

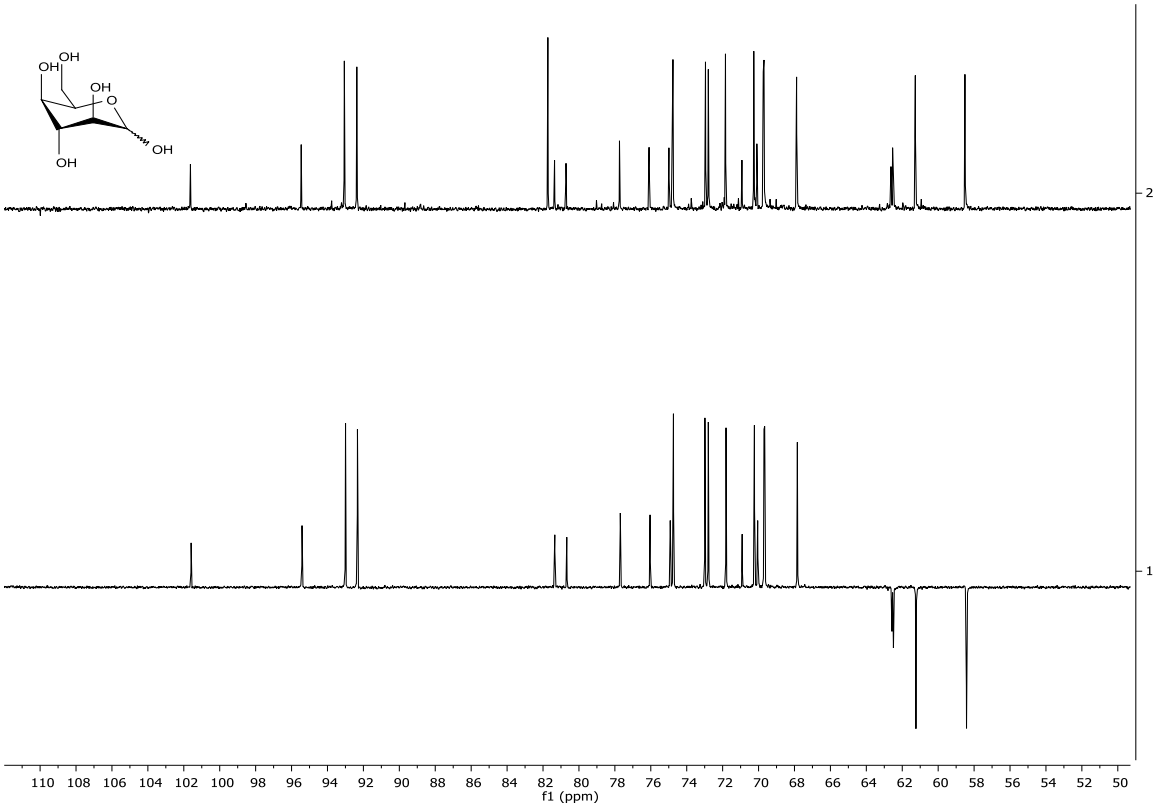

Figure S51. Comparison of ^{1}H-NMR of synthesized (top) and a commercial (bottom) D-talose **20**

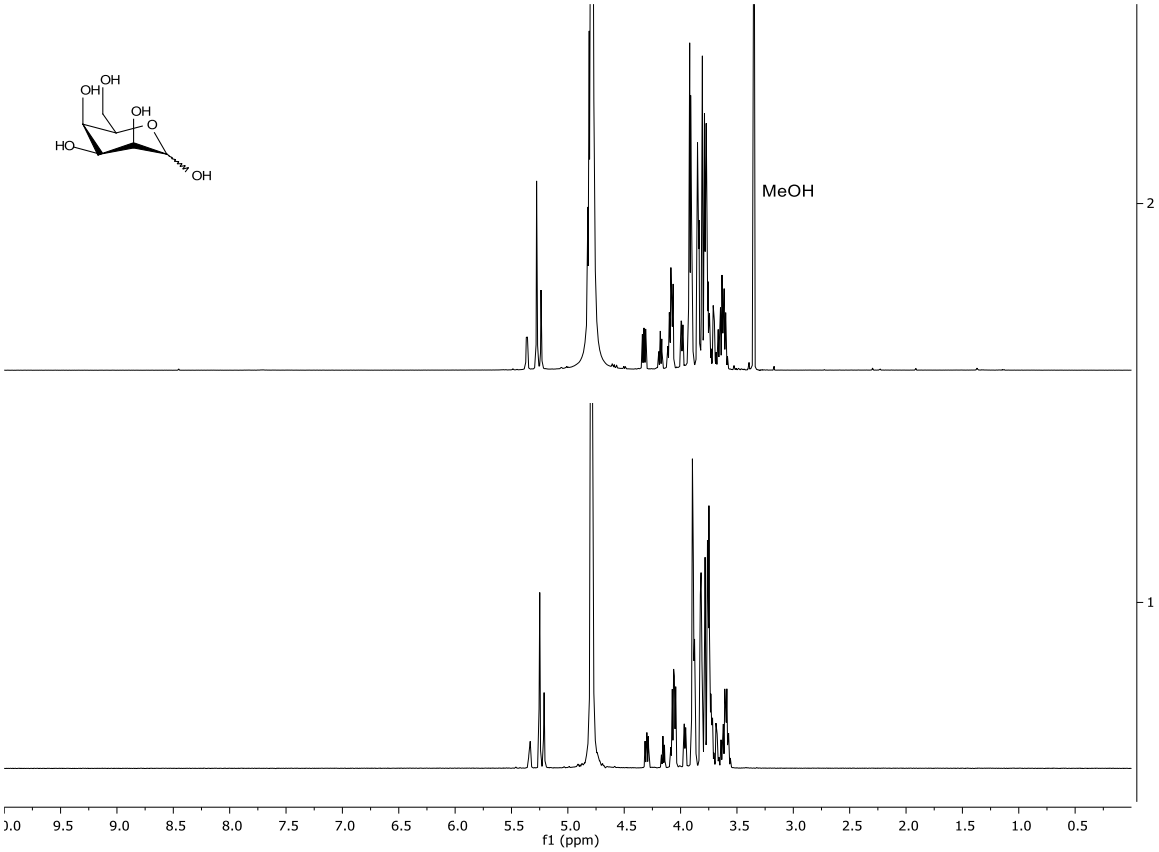

Figure S52. Comparison of ^{13}C-NMR of synthesized (top) and a commercial (bottom) D-talose **20**

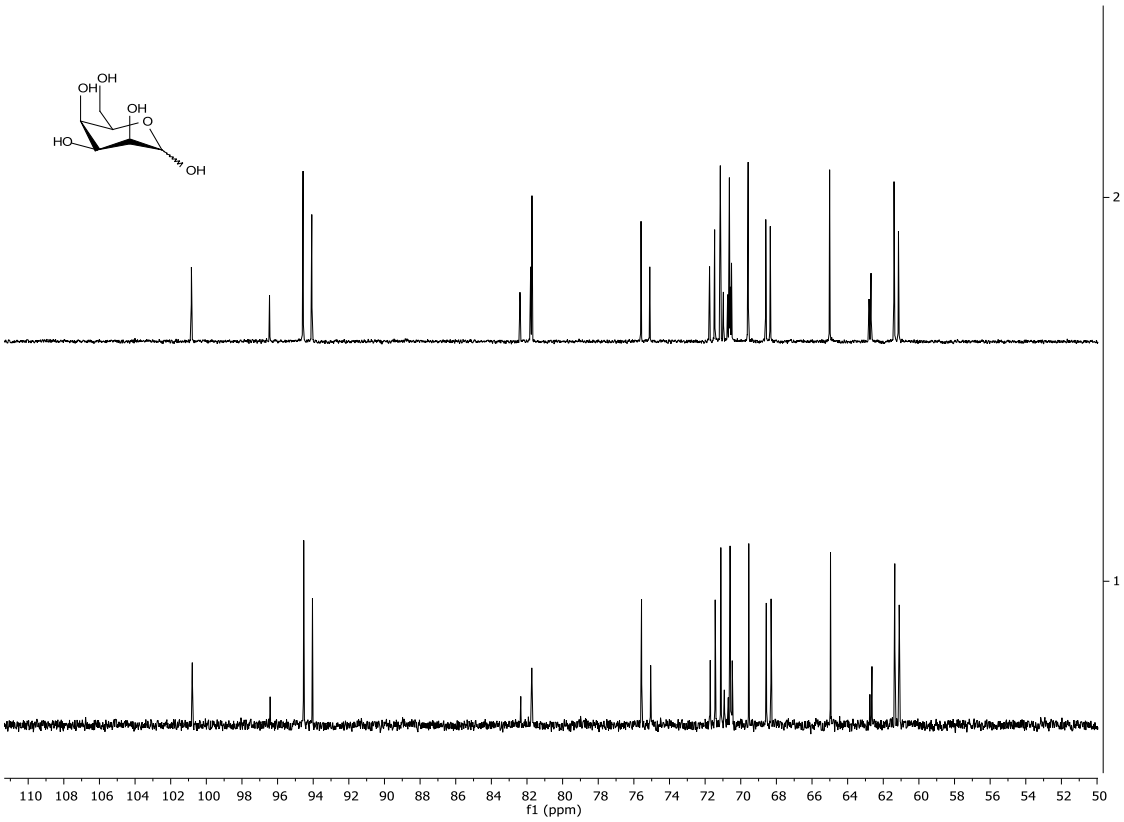

Figure S53. Comparison of ^{1}H-NMR of a synthesized mixture of D-galactose and D-talose (top) and commercially available D-galactose **21** (bottom)

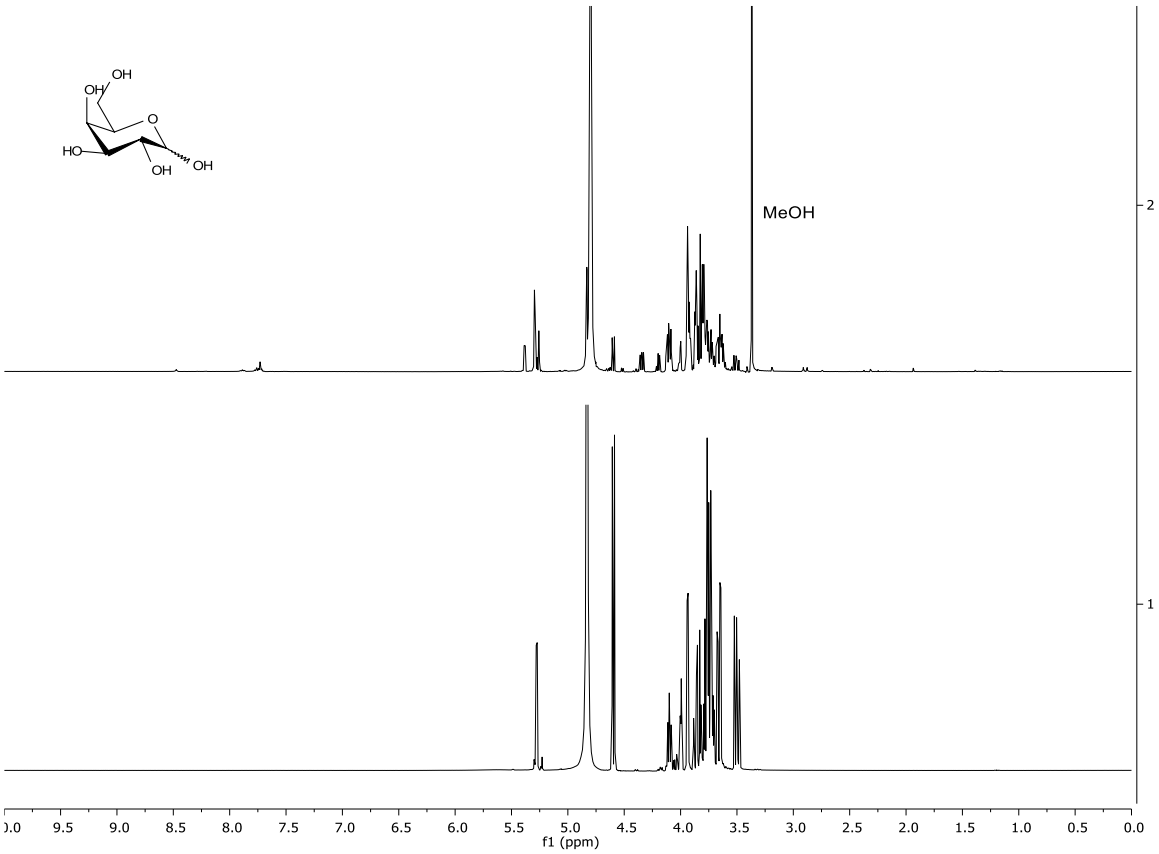

Figure S54. Comparison of ^{13}C-NMR of a synthesized mixture (middle) and commercially available D-galactose **21** (top) and D-talose **20** (bottom)